LETTER

doi:10.1038/nature25486

Mitochondria–lysosome contacts regulate mitochondrial fission via RAB7 GTP hydrolysis

Yvette C. Wong[1], Daniel Ysselstein[1] & Dimitri Krainc[1]

Both mitochondria and lysosomes are essential for maintaining cellular homeostasis, and dysfunction of both organelles has been observed in multiple diseases[1–4]. Mitochondria are highly dynamic and undergo fission and fusion to maintain a functional mitochondrial network, which drives cellular metabolism[5]. Lysosomes similarly undergo constant dynamic regulation by the RAB7 GTPase[1], which cycles from an active GTP-bound state into an inactive GDP-bound state upon GTP hydrolysis. Here we have identified the formation and regulation of mitochondria–lysosome membrane contact sites using electron microscopy, structured illumination microscopy and high spatial and temporal resolution confocal live cell imaging. Mitochondria–lysosome contacts formed dynamically in healthy untreated cells and were distinct from damaged mitochondria that were targeted into lysosomes for degradation[6,7]. Contact formation was promoted by active GTP-bound lysosomal RAB7, and contact untethering was mediated by recruitment of the RAB7 GTPase-activating protein TBC1D15 to mitochondria by FIS1 to drive RAB7 GTP hydrolysis and thereby release contacts. Functionally, lysosomal contacts mark sites of mitochondrial fission, allowing regulation of mitochondrial networks by lysosomes, whereas conversely, mitochondrial contacts regulate lysosomal RAB7 hydrolysis via TBC1D15. Mitochondria–lysosome contacts thus allow bidirectional regulation of mitochondrial and lysosomal dynamics, and may explain the dysfunction observed in both organelles in various human diseases.

Mitochondrial fission has multiple roles including mitochondrial biogenesis and mitochondrial DNA synthesis[5,8], and is regulated by the GTPase dynamin-related protein (DRP1), the endoplasmic reticulum, dynamin-2 and actin[9–16]. By contrast, lysosomal dynamics are regulated by GTP-bound active RAB7, which is recruited to late endosomal–lysosomal membranes but dissociates upon RAB GAP (GTPase-activating protein)-mediated GTP hydrolysis to become inactive, GDP-bound, and cytosolic[1,17]. Contact sites between mitochondria and lysosomes could thus provide a potential cellular mechanism for simultaneously regulating these dynamics.

Contacts between mitochondria and melanosomes, multi-vesicular bodies and yeast vacuoles have previously been studied[7,18–20]. Here, we identified contact sites between mitochondria and lysosomes in mammalian cells by performing electron microscopy on untreated HeLa cells. Mitochondria and lysosomes formed contacts (Fig. 1a and Extended Data Fig. 1a–c, yellow arrows) with an average distance between membranes of 9.57 ± 0.76 nm, consistent with other contact sites[21,22], and contact length of 198.33 ± 16.73 nm ($n = 55$ contacts from 20 cells; Fig. 1b). Using correlative light electron microscopy (CLEM), we confirmed that lysosomes or late endosomes positive for the acidic organelle label LysoTracker Red contained ultrastructure electron-dense lumens with irregular content and/or multilamellar membrane sheets (Extended Data Fig. 1d) and could simultaneously contact mitochondria and the endoplasmic reticulum (Extended Data Fig. 1e). Three-dimensional super-resolution structured illumination microscopy (N-SIM) of endogenous LAMP1 on late endosomal–lysosomal membranes, and TOM20 on outer mitochondrial membranes, further demonstrated that mitochondria–lysosome contacts spanned more than 200 nm in the *Z*-plane ($n = 210$ examples from 26 cells; Fig. 1c (left) and Extended Data Fig. 1f).

We next examined mitochondria–lysosome contacts in live cells using super-resolution N-SIM, and found that vesicles positive for LAMP1 labelled with mGFP (LAMP1–mGFP) and mitochondria expressing TOM20 labelled with mApple (mApple–TOM20) formed contacts in living HeLa cells (Fig. 1c, right). Using confocal microscopy at high spatial and temporal resolutions, mitochondria were found to contact both small (vesicle diameter $<0.5\,\mu$m) and larger (vesicle diameter $>1\,\mu$m) LAMP1 vesicles (Extended Data Fig. 2a, b), and LAMP1 vesicles could simultaneously contact multiple mitochondria (Extended Data Fig. 2c) and vice versa (Extended Data Fig. 2d). We also observed multiple examples of mitochondria–lysosome contacts stained for endogenous LAMP1 and TOM20 under confocal microscopy ($n = 341$ examples from 25 cells; Extended Data Fig. 2e).

LAMP1 vesicles and mitochondria remained in stable contact over time (Fig. 1d–g, yellow arrows; Supplementary Video 1), with LAMP1 vesicles approaching mitochondria to form stable contacts (Fig. 1h, yellow arrows), but eventually leaving mitochondria (white arrow) without engulfing them (Extended Data Fig. 2f, g). Contacts observed by confocal microscopy and live cell N-SIM lasted for 10 s or more (Fig. 1i and Extended Data Fig. 3a–c), with about 15% of LAMP1 vesicles in the cell contacting mitochondria at any given time (Fig. 1j). Furthermore, sensitized emission fluorescence resonance energy transfer (SE-FRET) was observed between TOM20–Venus (outer mitochondrial membrane) and LAMP1–mTurquoise2 (lysosomal membrane) at mitochondria–lysosome contacts (Extended Data Fig. 3d, e), further confirming the formation of these contacts in living cells.

Next, we analysed whether mitochondria–lysosome contacts represent sites of bulk protein transfer or mitochondrial degradation, either directly through mitochondrial-derived vesicles (MDVs) fusing with lysosomes[7] or indirectly through mitophagy[6]. Intermembrane space mitochondrial proteins and mitochondrial matrix proteins (Fig. 1k and Extended Data Fig. 4a–f) were not bulk transferred into lysosomes, and conversely, lysosomal luminal content marked by dextran was not bulk transferred into mitochondria at contact sites (Fig. 1k and Extended Data Fig. 4g–i). Moreover, mitochondria in contact with lysosomes were substantially larger (over 500 nm) than MDVs (about 100 nm)[7] and contained mitochondrial matrix proteins (Fig. 1k and Extended Data Fig. 4d–f), distinct from previously described TOM20-positive MDVs[23]. Mitochondria contacting lysosomes also did not undergo mitophagy, as they were not engulfed by LC3-positive autophagosomes (Extended Data Fig. 4j) or positive for autophagosome biogenesis markers (Extended Data Fig. 4k), suggesting that mitochondria–lysosome contacts do not lead to the bulk transfer of organelle luminal content or bulk mitochondrial degradation.

We then investigated whether mitochondria–lysosome contacts might be modulated by the lysosomal regulator RAB7 GTPase[1]. In

[1]Department of Neurology, Northwestern University Feinberg School of Medicine, Chicago, Illinois 60611, USA.

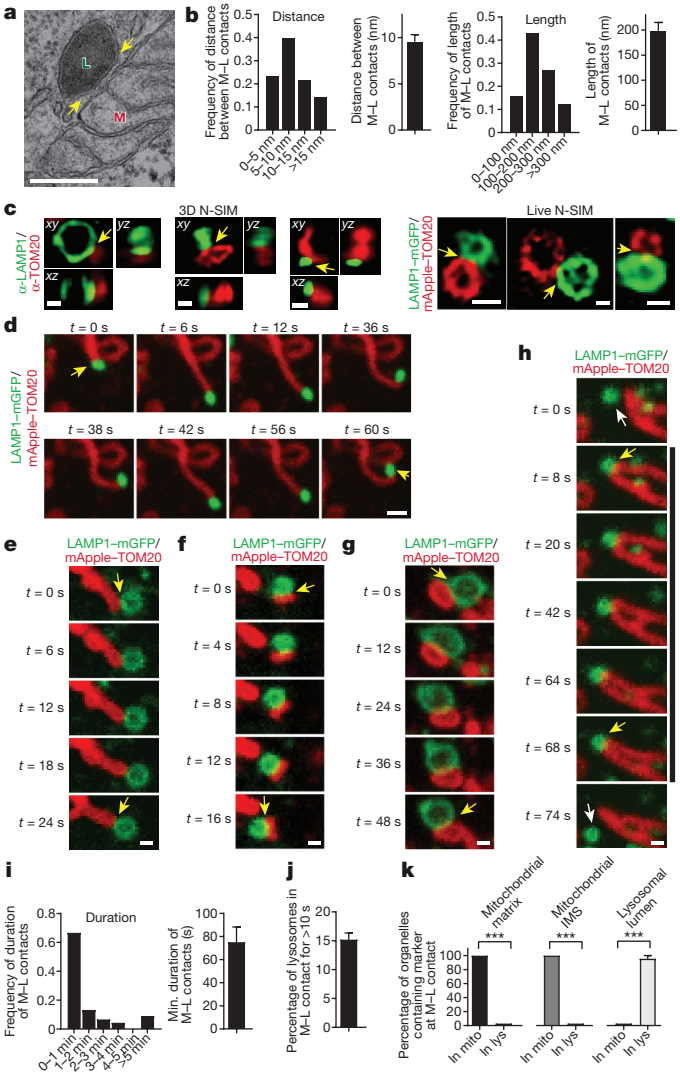

Figure 1 | Mitochondria and lysosomes form stable membrane contact sites. a, **b**, Representative electron microscopy image of mitochondria (M) and lysosome (L) contact (yellow arrows) in untreated HeLa cells (**a**) and quantification of distance between contact membranes and length of contact (**b**, $n = 55$ examples from 20 cells). **c**, Representative structured illumination microscopy (N-SIM) images of mitochondria–lysosome contacts (yellow arrows) in fixed HeLa cells stained for endogenous LAMP1 (lysosome) and TOM20 (mitochondria) and imaged in *Z*-stacks showing contacts extending more than 200 nm in the *Z*-plane (3D N-SIM; left; $n = 210$ examples from 26 cells) and in living HeLa cells expressing LAMP1–mGFP and mApple–TOM20 (live N-SIM; right; $n = 43$ examples from 10 cells). **d**–**h**, Representative time-lapse confocal images of stable mitochondria–lysosome contacts (yellow arrows) in living HeLa cells expressing LAMP1–mGFP (lysosomes) and mApple–TOM20 (mitochondria) ($n = 67$ examples from 23 cells). White arrows in **h** mark lysosomes before or after contact tethering to mitochondria. Black line shows duration of contact. **i**, **j**, Quantification of duration of mitochondria–lysosome contacts (**i**) and percentage of lysosomes contacting mitochondria (for >10 s; **j**) from confocal time-lapse images ($n = 45$ examples from 10 cells). **k**, Quantification of percentage of mitochondria (TOM20) or lysosomes (LAMP1) positive for mitochondrial matrix protein (mito–BFP; $n = 104$ events from 23 cells), mitochondrial intermembrane space (IMS) protein (SMAC–EGFP; $n = 57$ examples from 12 cells), or lysosomal lumen marker (pulse-chased dextran; $n = 66$ events from 18 cells) at mitochondria-lysosome contacts in living HeLa cells. Data are means ± s.e.m. (***$P < 0.0001$, unpaired two-tailed *t*-test). Scale bars, 200 nm (**a**); 500 nm (**c**, 3D N-SIM); 500 nm (**c**, Live N-SIM; left, right); 100 nm (**c**, Live N-SIM; middle); 1 μm (**d**); 0.5 μm (**e**–**h**).

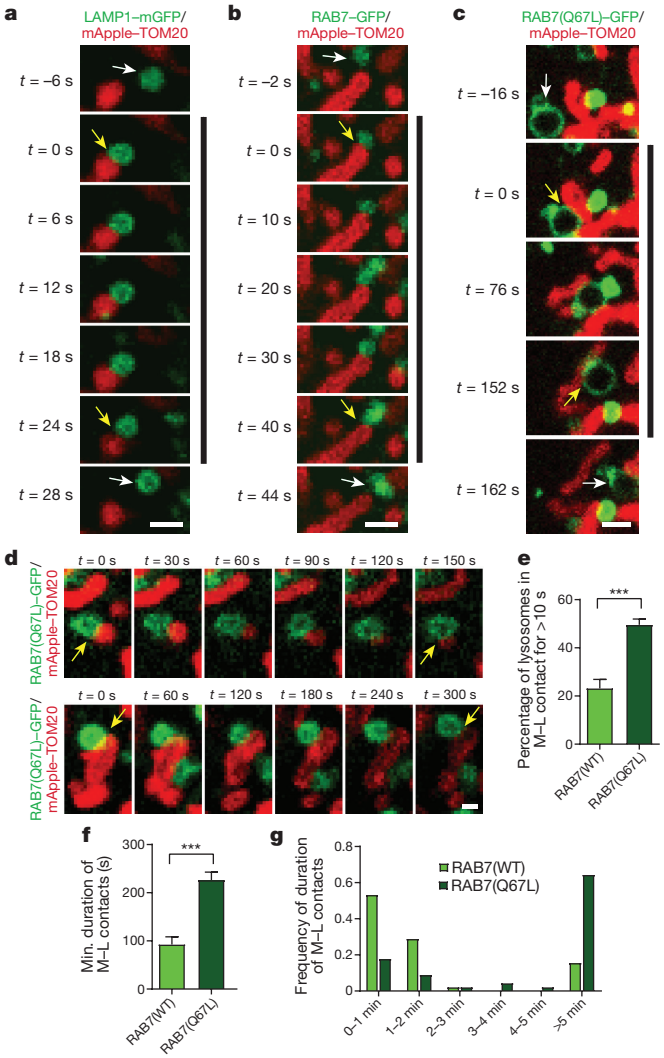

Figure 2 | RAB7 GTP hydrolysis promotes mitochondria–lysosome contact untethering. a–**c**, Representative time-lapse images of lysosome in cytosol (white arrow; top) approaching mitochondria to form a stable contact (yellow arrows; black line) before leaving mitochondria (white arrow; bottom) in living HeLa cells expressing mApple–TOM20 (mitochondria) and lysosomal markers LAMP1–mGFP (**a**), RAB7–GFP (**b**) or constitutively active GTP-bound RAB7(Q67L)–GFP mutant unable to undergo GTP hydrolysis (**c**) ($n = 45$ events from 9 cells per condition). **d**, Representative time-lapse images of mitochondria–lysosome contacts (yellow arrows) lasting more than 150 s in RAB7(Q67L)–GFP cells ($n = 45$ events from 9 cells). **e**–**g**, Expression of RAB7(Q67L) mutant leads to increased percentage of lysosomes in contacts ($n = 12$ cells per condition), and increased minimum duration of mitochondria–lysosome contacts ($n = 45$ events from 9 cells per condition). Data are means ± s.e.m. (***$P < 0.0001$, unpaired two-tailed *t*-test). Scale bars, 1 μm (**a**–**c**); 0.5 μm (**d**).

contrast to LAMP1–mGFP (Fig. 2a; Supplementary Video 2) or wild-type RAB7–GFP (Fig. 2b), expression of constitutively active GTP-bound mutant RAB7(Q67L)–GFP (Fig. 2c,d; Supplementary Video 3), which localized to lysosomal membranes, markedly increased both the percentage of lysosomes forming stable contacts with mitochondria (Fig. 2e) and mitochondria–lysosome contact duration ($n = 45$ events per condition; Fig. 2f, g). RAB7(Q67L) further resulted in a twofold increase in TOM20–LAMP1 mitochondria–lysosome FRET intensity compared to wild-type RAB7 ($n = 200$ cells per condition; Extended Data Fig. 3f), suggesting that GTP-bound RAB7 promotes contact formation whereas RAB7 GTP hydrolysis may be required for mitochondria–lysosome contact untethering.

We next examined how RAB7 GTP hydrolysis might be regulated at mitochondria–lysosome contacts. TBC1D15 is a RAB7 GAP that is recruited to mitochondria by the mitochondrial protein FIS1[24,25] to drive RAB7 GTP hydrolysis[26,27], potentially allowing mitochondria to regulate both contact untethering and lysosomal RAB7 hydrolysis via TBC1D15. Consistent with previous studies[24,25], mitochondrial localization of TBC1D15 was dependent on FIS1 binding (Extended Data Fig. 5a, d–f) but not inhibited by TBC1D15 mutants lacking GAP activity (D397A or R400K in the TBC domain)[25] (Extended Data Fig. 5b, c, e). Moreover, expression of mutant TBC1D15 could induce abnormally large lysosomes (Extended Data Fig. 5g), characteristic of inhibiting RAB7 GTP hydrolysis.

Using live cell time-lapse imaging, we found that the GAP mutants TBC1D15(D397A) (Fig. 3a, b and Extended Data Fig. 6a, b; Supplementary Video 4) and TBC1D15(R400K) (Fig. 3c) markedly increased mitochondria–lysosome contact duration compared to wild-type TBC1D15 ($n = 34$–38 events per condition; Fig. 3d, e) but did not alter the percentage of lysosomes forming contacts with mitochondria (Extended Data Fig. 6c). *TBC1D15*$^{-/-}$ HCT116 cells, generated using transcription activator-like effector nucleases (TALENs) and previously characterized[24], also showed a similar increase in contact duration, but no change in contact formation (Extended Data Fig. 6d, e), suggesting that RAB7 GTP hydrolysis induced by TBC1D15 does not regulate contact formation, but rather regulates contact duration by promoting contact untethering upon GTP hydrolysis.

Contact untethering was further dependent on the mitochondrial localization of TBCD15, as expression of a FIS1(LA) mutant that cannot recruit TBC1D15 to mitochondria[25] (Extended Data Fig. 5f) also induced abnormally enlarged lysosomes that contacted mitochondria (Fig. 3f), resulting in an increase in the duration and number of mitochondria–lysosome contacts (Fig. 3f, g and Extended Data Fig. 6f). Consistent with these findings, *FIS1*$^{-/-}$ HCT116 cells[24] also showed similar increases in contact duration and number (Extended Data Fig. 6g, h). However, localization of TBC1D15, FIS1 or RAB7 was not restricted to or concentrated at mitochondria–lysosome contact sites (Fig. 2b and Extended Data Fig. 6i,j). Together, these results suggest that RAB7 GTP hydrolysis is regulated at mitochondria–lysosome contacts by the GAP activity of TBC1D15, which is recruited to mitochondria by FIS1. Inhibition of RAB7 GTP hydrolysis leads to both defective lysosomal morphology and mitochondria–lysosome contacts that are unable to untether, and consequently remain in contact for a longer duration.

Finally, we investigated whether mitochondria–lysosome contacts also regulate mitochondrial dynamics. Time-lapse confocal microscopy showed that mitochondria underwent fission events at an average of 1.44 events per min in live HeLa cells. Unexpectedly, sites of mitochondrial fission were predominantly marked by a LAMP1 vesicle (yellow arrow) before the fission event (white arrows) (Fig. 4a–c, Extended Data Fig. 7a–c, Supplementary Videos 5, 6). LAMP1 vesicles contacted mitochondria at 81.5% of mitochondrial fission sites ($n = 44/54$ events from 18 cells), which was significantly greater than expected by random chance (12.6%; $***P < 0.0001$, Fisher's exact test; Fig. 4d) and greater than the percentage of contacts made by other vesicles such as early endosomes (GFP–EEA1) or peroxisomes (mEmerald–peroxisome) (<20% of fission events) (Fig. 4e). LAMP1 vesicles also localized to mitochondrial fission events at similar rates in other cell types including H4 neuroglioma, HEK293 and HCT116 cells (Extended Data Fig. 7d–g) and upon induction of mitochondrial fragmentation using actinomycin D, staurosporine (STS) or carbonyl cyanide m-chlorophenylhydrazone (CCCP) (Extended Data Fig. 8a–d). Mitochondrial fission events marked by lysosomes were also positive for mCherry–DRP1 oligomerization (Extended Data Fig. 9a) and endoplasmic reticulum tubules labelled with the endoplasmic reticulum markers mCherry–ER (100%; $n = 54/54$ events from 16 cells; Extended Data Fig. 9b, c), BFP–KDEL (100%; $n = 24/24$ events from 13 cells) or GFP–SEC61β (100%; $n = 11/11$ events from 11 cells), demonstrating

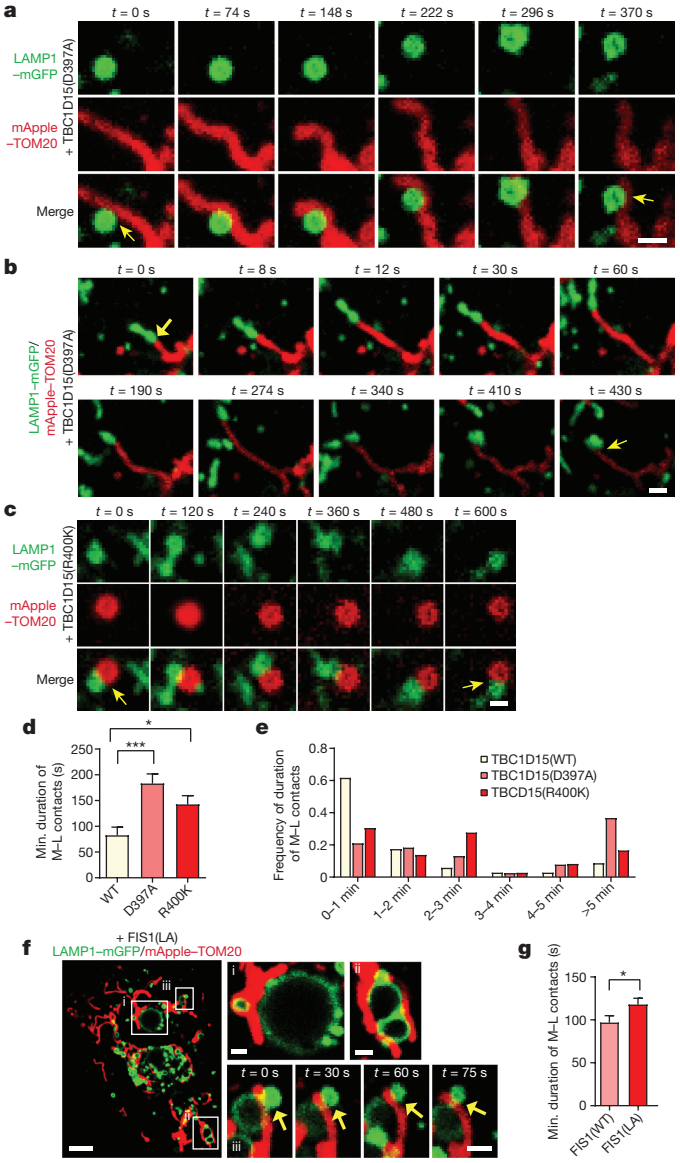

Figure 3 | Mitochondrial recruitment of TBC1D15, a RAB7 GAP, by FIS1 drives RAB7 GTP hydrolysis to promote mitochondria–lysosome contact untethering. a–c, Representative time-lapse images of stable mitochondria–lysosome contacts (yellow arrows) lasting more than 300 s in living HeLa cells expressing mApple–TOM20 (mitochondria), LAMP1–mGFP (lysosome) and TBC domain mutants TBC1D15(D397A) or TBC1D15(R400K) lacking GAP activity. **d**, Quantification of minimum duration of mitochondria–lysosome contacts, which are increased by TBC domain mutants compared to wild-type TBC1D15 ($n = 34$ events from 12 cells, wild-type; $n = 38$ events from 10 cells, D397A; $n = 36$ events from 11 cells, R400K). $*P = 0.0404$, $***P = 0.0002$; ANOVA with Tukey's post-hoc test. **e**, Duration frequencies of mitochondria–lysosome contacts. **f, g**, Expression of a FIS1(LA) mutant (unable to recruit TBC1D15 to mitochondria) leads to an increase in the minimum duration of mitochondria–lysosome contacts compared to wild-type FIS1 ($n = 45$ events from 9 cells per condition). $*P = 0.049$, unpaired two-tailed *t*-test. Data are means ± s.e.m. Scale bars, 1 μm (**a**, **b**); 0.5 μm (**c**); 5 μm (**f**); 1 μm (**f**, insets).

that mitochondria–lysosome contacts mark the sites of DRP1- and endoplasmic reticulum-positive mitochondrial fission events.

As RAB7 GTP hydrolysis regulates mitochondria–lysosome contacts, we investigated whether it also regulates mitochondrial fission. Expression of RAB7(Q67L) markedly reduced the rate of mitochondrial fission (Fig. 4f), resulting in mitochondria that did not undergo fission over time (Extended Data Fig. 10a). In addition, both the GAP

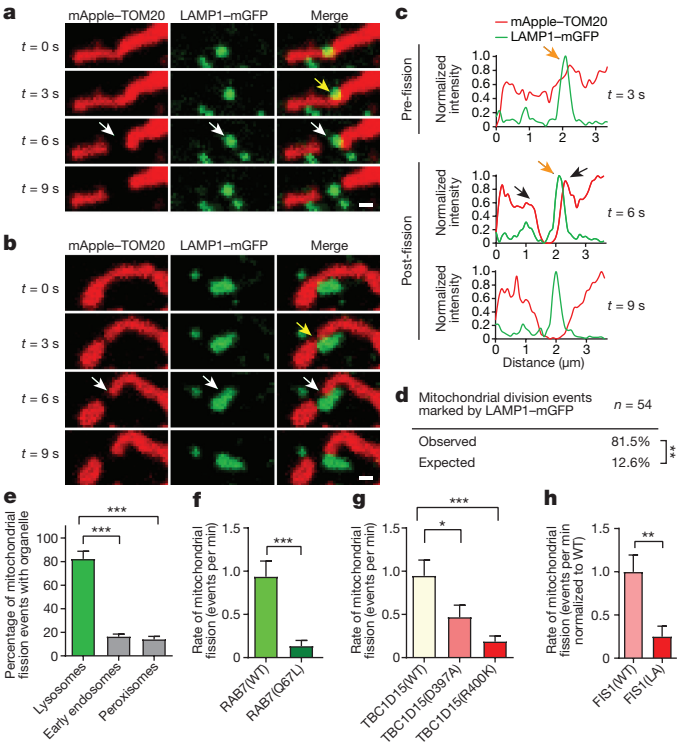

Figure 4 | Mitochondria–lysosome contacts mark sites of mitochondrial fission regulated by RAB7 GTP hydrolysis. a, **b**, Representative time-lapse images of lysosomes contacting mitochondria at the site of mitochondrial division (yellow arrow) before fission (white arrows) in living HeLa cells expressing LAMP1–mGFP (lysosomes) and mApple–TOM20 (mitochondria) ($n = 62$ events from 23 cells). **c**, Linescan corresponding to Fig. 4a showing a lysosome contacting a mitochondrion pre-fission (yellow arrow; top) and remaining in contact post-fission (yellow arrow; middle) after the mitochondria has divided into two daughter mitochondria (grey arrows; middle). **d**, **e**, Percentage of mitochondrial division events marked by LAMP1 vesicles in living HeLa cells expressing LAMP1–mGFP (lysosomes) and mApple–TOM20 (mitochondria) ($n = 54$ events from 18 cells). Significantly more events were marked by LAMP1 vesicles (81.5%) than expected by random chance (12.6%; $***P < 0.0001$, Fisher's exact test), or by early endosomes (GFP–EEA1) ($n = 45$ events from 17 cells; $***P < 0.0001$) or peroxisomes (mEmerald–peroxisome) ($n = 49$ events from 17 cells; $***P < 0.0001$). **f**–**h**, RAB7(Q67L) GTP-hydrolysis deficient mutant ($n = 10$ cells, RAB7; $n = 13$ cells, RAB7(Q67L); $***P = 0.0008$), TBC1D15 GAP mutants (D397A or R400K) ($n = 13$ cells per condition; $*P = 0.451$, $***P = 0.001$) or FIS1 (LA) mutant (unable to bind TBC1D15) ($n = 19$ cells, FIS1(WT); $n = 18$ cells, FIS1(LA); $**P = 0.0027$) lead to decreased rates of mitochondrial fission. Data are means ± s.e.m. ANOVA with Tukey's post-hoc test (**e**, **g**), unpaired two-tailed *t*-test (**f**, **h**). Scale bars, 0.5 μm (**a**, **b**).

mutants TBC1D15(D397A) and TBC1D15(R400K) (Fig. 4g, Extended Data Fig. 10b–e), and FIS1(LA), which disrupts TBC1D15 mitochondrial recruitment (Fig. 4h), markedly reduced mitochondrial fission rates. However, for the few fission events that did occur, the percentage of mitochondrial fission marked by lysosomes or endoplasmic reticulum was not altered by RAB7(Q67L) (Extended Data Fig. 10f, g) or TBC1D15 mutants (Extended Data Fig. 10h, i), further confirming that the majority of fission events are positive for lysosomes and endoplasmic reticulum. Moreover, inhibition of RAB7 GTP hydrolysis by RAB7(Q67L) or TBC1D15 GAP mutants reduced the percentage of cells with normal mitochondrial networks that were not hypertethered or overly elongated (Extended Data Fig. 10j–l). Thus, mitochondrial TBC1D15 recruited by FIS1 promotes RAB7 GTP hydrolysis at mitochondria–lysosome contacts to regulate both lysosomal morphology and mitochondrial fission.

In summary, we propose that mitochondria–lysosome contacts are regulated in two steps: formation and stabilization of contacts promoted by lysosomal GTP-bound RAB7, followed by contact untethering by TBC1D15, a RAB7 GAP recruited to mitochondria by FIS1, which drives RAB7 GTP hydrolysis at contact sites and results in dissociation of GDP-bound RAB7 from the membrane, which can no longer maintain stable contacts.

In addition, our work suggests that mitochondria–lysosome contacts regulate at least two important aspects of mitochondrial and lysosomal dynamics. First, lysosomal RAB7 hydrolysis is regulated by mitochondrial TBC1D15, providing a mechanism for mitochondria to modulate lysosomal dynamics by shutting down active RAB7, which regulates lysosomal transport, fusion and maturation[1]. Of note, the distance between TBC1D15's mitochondrial FIS1-binding site[25] and its TBC GAP domain for driving lysosomal RAB7 GTP hydrolysis is sufficient to span the distance (about 10 nm) between membranes at mitochondria–lysosome contact sites. This ability to regulate Rab GTP–GDP cycling on the opposing membrane of a target organelle may be similar to that proposed for GEF activation of the Golgi-localized RAB GTPase YPT1P by the TRAPPI complex on endoplasmic reticulum-derived COPII-coated vesicles[28].

Second, mitochondria–lysosome contacts mark sites of mitochondrial fission, conversely allowing lysosomal RAB7 to regulate mitochondrial dynamics. Previous studies examining the role of TBC1D15 in regulating mitochondrial morphology at steady state[24,25] and that of FIS1 in regulating the mitochondrial fission machinery have been controversial. Although our data suggest that both TBC1D15 and FIS1 indirectly regulate mitochondrial fission events via lysosomal RAB7 GTP hydrolysis, further work examining their mechanistic role in this process will be important. As membrane contact sites mediate multiple forms of inter-organelle communication[22,29], we hypothesize that mitochondria–lysosome contacts also function as platforms for metabolic exchanges between the two organelles. Thus, future studies of additional roles and protein tethers involved at these contacts will provide valuable insight into cellular organization and the pathogenesis of multiple diseases linked to both mitochondrial and lysosomal dysfunction[2–4,30].

Online Content Methods, along with any additional Extended Data display items and Source Data, are available in the online version of the paper; references unique to these sections appear only in the online paper.

Received 23 March 2017; accepted 3 January 2018.
Published online 24 January 2018.

1. Hutagalung, A. H. & Novick, P. J. Role of Rab GTPases in membrane traffic and cell physiology. *Physiol. Rev.* **91,** 119–149 (2011).
2. Burté, F., Carelli, V., Chinnery, P. F. & Yu-Wai-Man, P. Disturbed mitochondrial dynamics and neurodegenerative disorders. *Nat. Rev. Neurol.* **11,** 11–24 (2015).
3. Mc Donald, J. M. & Krainc, D. Lysosomal proteins as a therapeutic target in neurodegeneration. *Annu. Rev. Med.* **68,** 445–458 (2017).
4. Plotegher, N. & Duchen, M. R. Mitochondrial dysfunction and neurodegeneration in lysosomal storage disorders. *Trends Mol. Med.* **23,** 116–134 (2017).
5. Mishra, P. & Chan, D. C. Metabolic regulation of mitochondrial dynamics. *J. Cell Biol.* **212,** 379–387 (2016).
6. Pickrell, A. M. & Youle, R. J. The roles of PINK1, parkin, and mitochondrial fidelity in Parkinson's disease. *Neuron* **85,** 257–273 (2015).
7. Sugiura, A., McLelland, G. L., Fon, E. A. & McBride, H. M. A new pathway for mitochondrial quality control: mitochondrial-derived vesicles. *EMBO J.* **33,** 2142–2156 (2014).
8. Lewis, S. C., Uchiyama, L. F. & Nunnari, J. ER-mitochondria contacts couple mtDNA synthesis with mitochondrial division in human cells. *Science* **353,** aaf5549 (2016).
9. Smirnova, E., Griparic, L., Shurland, D. L. & van der Bliek, A. M. Dynamin-related protein Drp1 is required for mitochondrial division in mammalian cells. *Mol. Biol. Cell* **12,** 2245–2256 (2001).
10. Friedman, J. R. *et al.* ER tubules mark sites of mitochondrial division. *Science* **334,** 358–362 (2011).
11. Korobova, F., Ramabhadran, V. & Higgs, H. N. An actin-dependent step in mitochondrial fission mediated by the ER-associated formin INF2. *Science* **339,** 464–467 (2013).

12. Ji, W. K., Hatch, A. L., Merrill, R. A., Strack, S. & Higgs, H. N. Actin filaments target the oligomeric maturation of the dynamin GTPase Drp1 to mitochondrial fission sites. *eLife* **4,** e11553 (2015).
13. Li, S. *et al.* Transient assembly of F-actin on the outer mitochondrial membrane contributes to mitochondrial fission. *J. Cell Biol.* **208,** 109–123 (2015).
14. Manor, U. *et al.* A mitochondria-anchored isoform of the actin-nucleating spire protein regulates mitochondrial division. *eLife* **4,** (2015).
15. Moore, A. S., Wong, Y. C., Simpson, C. L. & Holzbaur, E. L. Dynamic actin cycling through mitochondrial subpopulations locally regulates the fission–fusion balance within mitochondrial networks. *Nat. Commun.* **7,** 12886 (2016).
16. Lee, J. E., Westrate, L. M., Wu, H., Page, C. & Voeltz, G. K. Multiple dynamin family members collaborate to drive mitochondrial division. *Nature* **540,** 139–143 (2016).
17. Zhen, Y. & Stenmark, H. Cellular functions of Rab GTPases at a glance. *J. Cell Sci.* **128,** 3171–3176 (2015).
18. Daniele, T. *et al.* Mitochondria and melanosomes establish physical contacts modulated by Mfn2 and involved in organelle biogenesis. *Curr. Biol.* **24,** 393–403 (2014).
19. Elbaz-Alon, Y. *et al.* A dynamic interface between vacuoles and mitochondria in yeast. *Dev. Cell* **30,** 95–102 (2014).
20. Hönscher, C. *et al.* Cellular metabolism regulates contact sites between vacuoles and mitochondria. *Dev. Cell* **30,** 86–94 (2014).
21. Csordás, G. *et al.* Structural and functional features and significance of the physical linkage between ER and mitochondria. *J. Cell Biol.* **174,** 915–921 (2006).
22. Phillips, M. J. & Voeltz, G. K. Structure and function of ER membrane contact sites with other organelles. *Nat. Rev. Mol. Cell Biol.* **17,** 69–82 (2016).
23. Soubannier, V. *et al.* A vesicular transport pathway shuttles cargo from mitochondria to lysosomes. *Curr. Biol.* **22,** 135–141 (2012).
24. Yamano, K., Fogel, A. I., Wang, C., van der Bliek, A. M. & Youle, R. J. Mitochondrial Rab GAPs govern autophagosome biogenesis during mitophagy. *eLife* **3,** e01612 (2014).
25. Onoue, K. *et al.* Fis1 acts as a mitochondrial recruitment factor for TBC1D15 that is involved in regulation of mitochondrial morphology. *J. Cell Sci.* **126,** 176–185 (2013).
26. Peralta, E. R., Martin, B. C. & Edinger, A. L. Differential effects of TBC1D15 and mammalian Vps39 on Rab7 activation state, lysosomal morphology, and growth factor dependence. *J. Biol. Chem.* **285,** 16814–16821 (2010).
27. Zhang, X. M., Walsh, B., Mitchell, C. A. & Rowe, T. TBC domain family, member 15 is a novel mammalian Rab GTPase-activating protein with substrate preference for Rab7. *Biochem. Biophys. Res. Commun.* **335,** 154–161 (2005).
28. Cai, H. *et al.* TRAPPI tethers COPII vesicles by binding the coat subunit Sec23. *Nature* **445,** 941–944 (2007).
29. Eisenberg-Bord, M., Shai, N., Schuldiner, M. & Bohnert, M. A tether is a tether is a tether: tethering at membrane contact sites. *Dev. Cell* **39,** 395–409 (2016).
30. Burbulla, L. F. *et al.* Dopamine oxidation mediates mitochondrial and lysosomal dysfunction in Parkinson's disease. *Science* **357,** 1255–1261 (2017).

Supplementary Information is available in the online version of the paper.

Acknowledgements We thank K. Trajkovic and all members of the Krainc laboratory for advice, F. Korobova for electron microscopy assistance and J. Z. Rappoport and D. Kirchenbuechler for N-SIM assistance. All imaging work was performed at the Northwestern University Center for Advanced Microscopy, supported by NCI CCSG P30 CA060553 awarded to the Robert H Lurie Comprehensive Cancer Center. Structured illumination microscopy was performed on a Nikon N-SIM system, purchased with the support of NIH 1S10OD016342-01. The spinning disk confocal system was acquired through a NCRR shared instrumentation grant awarded to V. Gelfand (S10 RR031680-01). *TBC1D15* and *FIS1* constructs were gifts from N. Ishihara. HCT116 wild-type and knockout cells were gifts from R. Youle. This work was supported by NIH/NINDS grants to Y.C.W. (T32 NS041234 and F32 NS101778) and D.K. (R01 NS076054).

Author Contributions Y.C.W. and D.K. designed the overall study, analysed data and wrote the manuscript. Y.C.W. performed cell culture, electron microscopy, correlative light electron microscopy, structured illumination microscopy, confocal live cell imaging and immunofluorescence. D.Y. designed, performed and analysed FRET experiments.

Author Information Reprints and permissions information is available at www.nature.com/reprints. The authors declare no competing financial interests. Readers are welcome to comment on the online version of the paper. Publisher's note: Springer Nature remains neutral with regard to jurisdictional claims in published maps and institutional affiliations. Correspondence and requests for materials should be addressed to D.K. (dkrainc@nm.org).

METHODS

No statistical methods were used to predetermine sample size. For studies involving multiple different experimental conditions in the same cell line, studies were performed on cells originating from the same cell line batch and randomly assigned experimental conditions for transfection. For preliminary analyses, researchers who were either involved or not involved in the study were asked to examine blinded samples for biological effects.

Reagents. The following plasmids were obtained from Addgene: LAMP1–mGFP was a gift from E. Dell'Angelica (Addgene #34831)[31], LAMP1–RFP was a gift from W. Mothes (Addgene #1817)[32], BFP–KDEL, mito–BFP, mCherry–Drp1 and mCherry–RAB7A were gifts from G. Voeltz (Addgene #49150, #49151, #49152, #61804)[10,33], EGFP–LC3 was a gift from K. Kirkegaard (Addgene #11546)[34], GFP–DFCP1 was a gift from N. Mizushima (Addgene #38269)[35], pAc-GFPC1–Sec61β was a gift from T. Rapoport (Addgene #15108), pCMV3-SMAC–HA–eGFP was a gift from R. Kahn (Addgene #67489), mVenus C1 was a gift from S. Vogel (Addgene #27794)[36], pK_anCMV–mClover3–mRuby3 was a gift from M. Lin (Addgene #74252)[37], EGFP–RAB7A(WT) and EGFP–RAB7A(Q67L) were gifts from Q. Zhong (Addgene #28047, #28049)[38], mTagBFP2–Lysosomes-20[39], mApple–TOMM20-N-10, mEmerald–TOMM20-C-10, DsRed2–Mito-7, mCherry–ATG5-C-18, mEmerald–ATG12-N-18, mCherry–ER-3, mEmerald–Peroxisome-2 and pmTurquoise2–N1 were gifts from M. Davidson (Addgene #55308, #54955, #54281, #55838, # 54995, # 54003, #55041, #54228, #60561) and GFP–EEA1 wild type was a gift from S. Corvera (Addgene #42307)[40]. N-terminal HA-tagged TBC1D15 plasmids (wild-type, D397A, R400K and Δ231–240) and Flag–FIS1 (wild-type and LA mutant) were gifts from N. Ishihara[25,41]. YFP–TBC1D15 was a gift from R. Youle[24]. ULK1–GFP was a gift from V. Deretic[42]. The following reagents were also used: dextran cascade blue 10000MW (Thermo Fisher Scientific; D1976), LAMP1 rabbit antibody (Sigma-Aldrich, L1418), TOM20 mouse antibody (BD biosciences, 612278), Flag rabbit antibody (Sigma-Aldrich, F7425), HA rabbit antibody (Cell Signaling, 3724S), HA mouse antibody (Cell Signaling, 2367S) and Alexa fluorophore-conjugated secondary antibodies from Molecular Probes (Invitrogen).

Cell culture and transfection. HeLa cells (gift from M. Schwake (ATCC)) and HEK293 cells (human embryonic kidney cell line 293FT (Life Technologies)) were cultured in Dulbecco's modified Eagle's medium (DMEM) (Gibco; 11995-065) supplemented with 10% (vol/vol) FBS, 100 units per ml penicillin, and 100 μg/ml streptomycin. Wild-type, *FIS1*$^{-/-}$ and *TBC1D15*$^{-/-}$ HCT116 cells were gifts from R. Youle[24] and cultured in McCoy's 5A with L-glutamine (ATCC 30-2007) supplemented with 10% (vol/vol) FBS, 100 units per ml penicillin, and 100 μg/ml streptomycin and nonessential amino acids. H4 neuroglioma cells[43] were cultured in Optimem + 5% FBS, 200 μg/ml geneticin and hygromycin and 1% penicillin/streptomycin (Life Technologies), and treated with 1 μg/ml doxycycline (Sigma) for 3 days. All cells were maintained at 37 °C in a 5% CO^2 incubator and previously verified by cytochrome *c* oxidase subunit I (COI) and short tandem repeat (STR) testing, and were tested and found negative for mycoplasma contamination. Cells were transfected using Lipofectamine 2000 (Invitrogen). Dextran blue was used at 1 mg/ml and pulsed via incubation in medium for 15 min and chased for 4 h, resulting in 95% of LAMP1-positive vesicles containing dextran blue by this time point. For drug treatments, live cells were imaged while being treated for 20 min with actinomycin D (10 μM) (Sigma-Aldrich; A9415), STS (1 μM) (Sigma-Aldrich; S6942) or CCCP (20 μM) (Sigma-Aldrich C2759). For live imaging, cells were grown on glass-bottomed culture dishes (MatTek; P35G-1.5-14-C).

Immunofluorescence. Cells were plated on coverslips and fixed in 3% (vol/vol) paraformaldehyde for 15 min and permeabilized with 2% BSA and 0.1% saponin. Fixed cells were incubated in primary antibody for 1 h, washed three times for 5 min each, incubated in secondary antibody for 1 h, washed three times for 5 min each, and mounted on glass slides with fluorescent mounting medium (Dako).

Confocal microscopy. All non-FRET confocal images were acquired on a Nikon A1R laser scanning confocal microscope with GaAsp detectors using a Plan Apo λ 100x 1.45 NA oil immersion objective (Nikon) using NIS-Elements (Nikon). Live cells were imaged in a temperature-controlled chamber (37 °C) at 5% CO_2 at 1 frame every 2–3 s. Dual-colour videos were acquired as consecutive green–red images, and tricolour videos were acquired as consecutive green–red–blue images.

Electron microscopy. For electron microscopy (EM), cells were grown on coverslips and fixed in a mixture of 2.5% glutaraldehyde and 2% paraformaldehyde in 0.1 M cacodylate buffer for 2–24 h at 4 °C. After post-fixation in 1% osmium tetroxide and 3% uranyl acetate, cells were dehydrated in an ethanol series, embedded in Epon resin and polymerized for 48 h at 60 °C. Ultrathin sections were made using a UCT ultramicrotome (Leica Microsystems) and contrasted with 4% uranyl acetate and Reynolds's lead citrate. Samples were imaged using a FEI Tecnai Spirit G2 transmission electron microscope (FEI) operated at 80 kV. Images were captured with an Eagle 4k HR 200kV CCD camera. For correlative light electron microscopy, cells were grown on gridded glass-bottom culture dishes (MatTek; P35G-1.5-14-CGRD) and incubated for 45 min with LysoTracker Red (2 μM) (Thermo Fisher Scientific) before EM fixation. Fixed cells were imaged on the Nikon A1R laser scanning confocal microscope for LysoTracker staining using *Z*-stacks with step sizes of 0.2 μm as described above, and subsequently processed and imaged for EM as described above.

Structured illumination microscopy. Structured illumination microscopy (SIM) super-resolution images were taken on a Nikon N-SIM system with a 100× oil immersion objective lens, 1.49 NA (Nikon). Images were captured using Nikon NIS-Elements and reconstructed using slice reconstruction in NIS-elements. Images for live cell imaging (live N-SIM) were taken at a single *Z*-plane, while images of fixed cells for 3D N-SIM were taken using *Z*-stacks with step sizes of 0.2 μm. Cells used for live cell imaging were maintained in a temperature-controlled chamber (37 °C) at 5% CO_2 in a TokaiHit stagetop incubator.

FRET pair generation, imaging and analysis. The outer mitochondrial membrane (TOM20–Venus) and lysosomal membrane (LAMP1–mTurquoise2) FRET pair was generated using mVenus C1 (Addgene #27794) and pmTurquoise2-N1 (Addgene #60561). mRuby3 and RAB7a(Q67L)–mRuby3 were generated using mRuby3 obtained from pK_anCMV–mClover3–mRuby3 (Addgene #74252)[37]. For FRET experiments, HeLa cells were plated on 35-mm 4-chamber glass-bottomed dishes (Cellvis) at a density of 40,000 cells per well. The following day, cells were transfected using lipofectamine with FRET pairs (TOM20–Venus and LAMP1–mTurquoise2) along with mRuby, RAB7a(WT)–mCherry or RAB7a(Q67L)–mRuby3. Images of live HeLa cells were acquired using a Nikon Spinning disk confocal microscope using 20× (for FRET intensity calculations) and 60× objectives (for representative time-lapse images) at excitation wavelengths of 445 nm, 515 nm, and 561 nm for mTurquoise2, Venus, and mCherry/mRuby3, respectively, in a temperature-controlled chamber (37 °C) at 5% CO_2 using NIS-Elements (Nikon). NIS-Elements (Nikon) was used for FRET analysis to calculate sensitized emission FRET (SE-FRET) and to unbiasedly generate regions of interest (ROI) by tracing individual cells in the red fluorescence view. A total of $n = 200$ cells were analysed per condition for RAB7a(WT) and RAB7a(Q67L) and the FRET intensity was normalized to average SE-FRET values for RAB7a(WT).

Image analysis. Mitochondrial fission events were defined as those that showed clear division of a single mitochondrion into two distinct daughter mitochondria that moved independently of one another after division. The expected probability that a LAMP1 vesicle would be at the site of a mitochondrial division event by random chance was calculated as the density of LAMP1 vesicles in the cytosol from $n = 26$ living cells, using ImageJ (National Institutes of Health (NIH)). Mitochondria–lysosome contacts imaged in living cells were categorized as those that showed mitochondria and lysosomes in close proximity (<0.1 μm) for >10 s in time-lapse images. All contacts analysed for the minimum duration of contacts were those that had already formed at the beginning of the video. The minimum duration of contact in HeLa cells was quantified as the time before contact termination and dissociation (mitochondria and lysosomes detaching from one another) over a 5-min (300-s) video. Any contacts that lasted throughout the entire 5-min video and were still in contact by the end of the video were categorized as 300 s in bar graphs and as >5 min in histograms for the minimum duration of mitochondria–lysosome contacts. The percentage of lysosomes in contacts was quantified as the percentage of vesicles that formed contacts (defined above) with mitochondria divided by the total number of vesicles in the region of interest. The minimum duration of contact in HCT116 cells was quantified from videos of ≥100 s. Mitochondrial networks that did not contain overly elongated mitochondria (>10 μm length) or hyperfused or hypertethered mitochondria were classified as normal and scored per condition. The rate of mitochondrial fission was calculated per cell by quantifying the number of fission events in the entire cell from videos of ≥100 s. The distance between membranes and the length of mitochondria–lysosome contact sites were measured from EM images using ImageJ (NIH). Line scans were generated using ImageJ (NIH) and normalized per protein.

Statistical analysis, graphing and figure assembly. Data were analysed using unpaired two-tailed Student *t*-test (for two datasets) or one-way ANOVA with Tukey's post hoc test (for multiple datasets). Fisher's exact test was used to compare the percentage of observed mitochondrial division events with mitochondria–lysosome contacts versus the percentage expected by random chance. Data presented are means ± s.e.m. (except in histograms). All statistical tests were justified as appropriate and were analysed from $n \geq 9$ cells (see text and figure legends for details) from $n \geq 3$ independent experiments (biological replicates) per condition. Statistics and graphing were performed using Prism 7 (GraphPad) software. All videos and images were assembled using ImageJ 1.51j8 (NIH). All final figures were assembled in Illustrator (Adobe).

Data Availability. All data that support the findings of this study are included in the manuscript or are available from the authors upon reasonable request.

31. Falcón-Pérez, J. M., Nazarian, R., Sabatti, C. & Dell'Angelica, E. C. Distribution and dynamics of Lamp1-containing endocytic organelles in fibroblasts deficient in BLOC-3. *J. Cell Sci.* **118,** 5243–5255 (2005).
32. Sherer, N. M. *et al.* Visualization of retroviral replication in living cells reveals budding into multivesicular bodies. *Traffic* **4,** 785–801 (2003).
33. Rowland, A. A., Chitwood, P. J., Phillips, M. J. & Voeltz, G. K. ER contact sites define the position and timing of endosome fission. *Cell* **159,** 1027–1041 (2014).
34. Jackson, W. T. *et al.* Subversion of cellular autophagosomal machinery by RNA viruses. *PLoS Biol.* **3,** e156 (2005).
35. Itakura, E. & Mizushima, N. Characterization of autophagosome formation site by a hierarchical analysis of mammalian Atg proteins. *Autophagy* **6,** 764–776 (2010).
36. Koushik, S. V., Chen, H., Thaler, C., Puhl, H. L. III & Vogel, S. S. Cerulean, Venus, and VenusY67C FRET reference standards. *Biophys. J.* **91,** L99–L101 (2006).
37. Bajar, B. T. *et al.* Improving brightness and photostability of green and red fluorescent proteins for live cell imaging and FRET reporting. *Sci. Rep.* **6,** 20889 (2016).
38. Sun, Q., Westphal, W., Wong, K. N., Tan, I. & Zhong, Q. Rubicon controls endosome maturation as a Rab7 effector. *Proc. Natl Acad. Sci. USA* **107,** 19338–19343 (2010).
39. Subach, O. M., Cranfill, P. J., Davidson, M. W. & Verkhusha, V. V. An enhanced monomeric blue fluorescent protein with the high chemical stability of the chromophore. *PLoS ONE* **6,** e28674 (2011).
40. Lawe, D. C., Patki, V., Heller-Harrison, R., Lambright, D. & Corvera, S. The FYVE domain of early endosome antigen 1 is required for both phosphatidylinositol 3-phosphate and Rab5 binding. Critical role of this dual interaction for endosomal localization. *J. Biol. Chem.* **275,** 3699–3705 (2000).
41. Jofuku, A., Ishihara, N. & Mihara, K. Analysis of functional domains of rat mitochondrial Fis1, the mitochondrial fission-stimulating protein. *Biochem. Biophys. Res. Commun.* **333,** 650–659 (2005).
42. Mandell, M. A. *et al.* TRIM proteins regulate autophagy and can target autophagic substrates by direct recognition. *Dev. Cell* **30,** 394–409 (2014).
43. Mazzulli, J. R. *et al.* Gaucher disease glucocerebrosidase and α-synuclein form a bidirectional pathogenic loop in synucleinopathies. *Cell* **146,** 37–52 (2011).

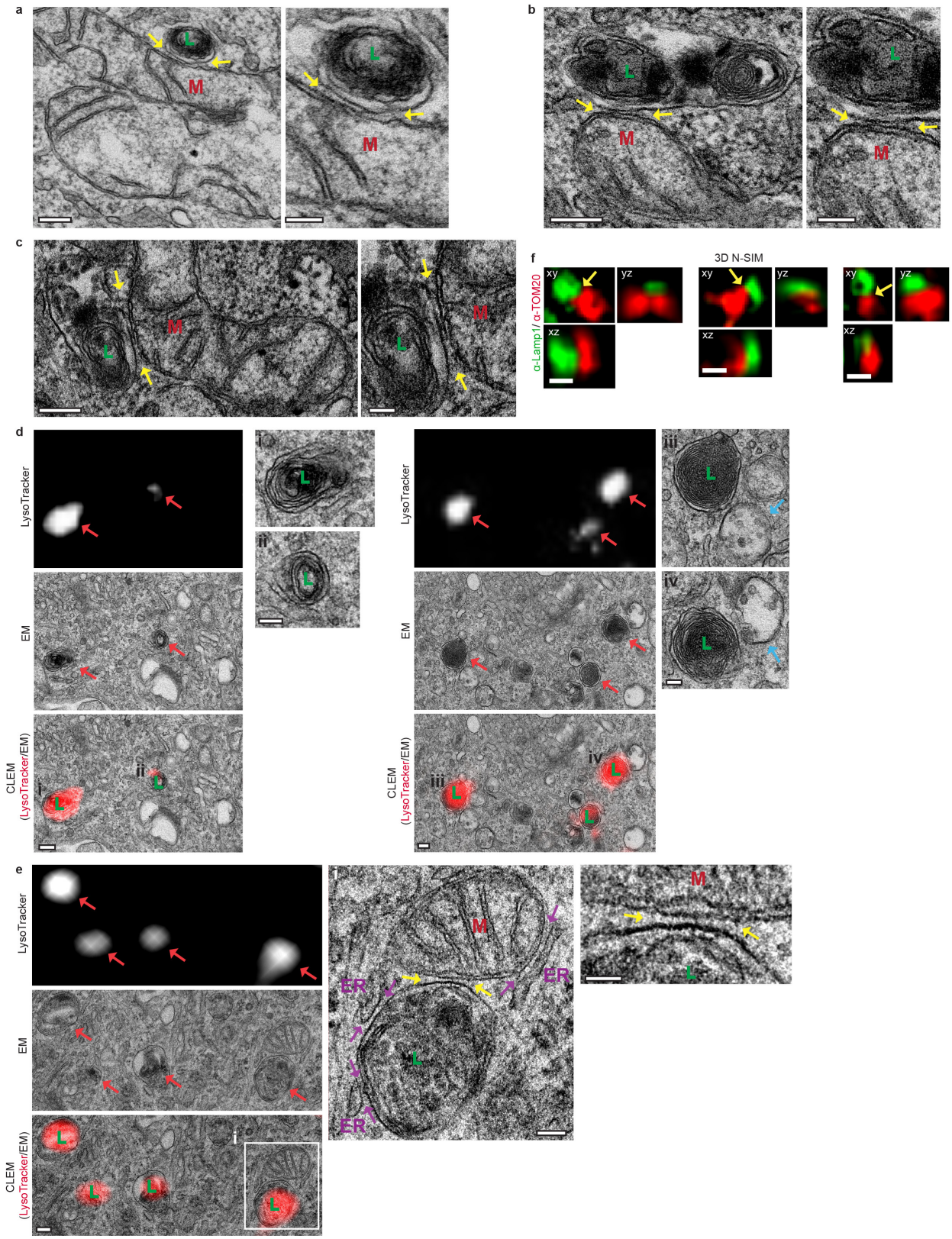

Extended Data Figure 1 | Correlative light electron microscopy and 3D structured illumination microscopy of mitochondria–lysosome contacts. a–c, Representative electron microscopy images of mitochondria (M) and lysosome (L) contacts (yellow arrows) in untreated HeLa cells (insets shown on right) ($n = 55$ examples from 20 cells). **d**, **e**, Representative correlative light electron microscopy and confocal images of HeLa cells (from $n = 14$ images from 6 cells) incubated with LysoTracker Red to label lysosomes or late endosomes (red arrows) that contain electron-dense lumen with irregular content and/or multilamellar membrane sheets (**d**, see insets on right), and form a stable membrane contact site with mitochondria (**e**, yellow arrows; see inset on right), while simultaneously forming contact sites with the endoplasmic reticulum (**e**, purple arrows). Early endosomes lacking electron-dense lumen are LysoTracker-negative (**d**, blue arrows). **f**, Representative structured illumination microscopy (N-SIM) images of mitochondria–lysosome contacts (yellow arrows) in fixed HeLa cells stained for endogenous LAMP1 (lysosomes) or TOM20 (mitochondria) and imaged in *Z*-stacks showing contacts extending more than 200 nm in the *Z*-plane ($n = 210$ examples from 26 cells). Scale bars, 200 nm (**a–d**); 100 nm (**a–d**, insets on right; **e**, left, middle); 50 nm (**e**, right); 500 nm (**f**).

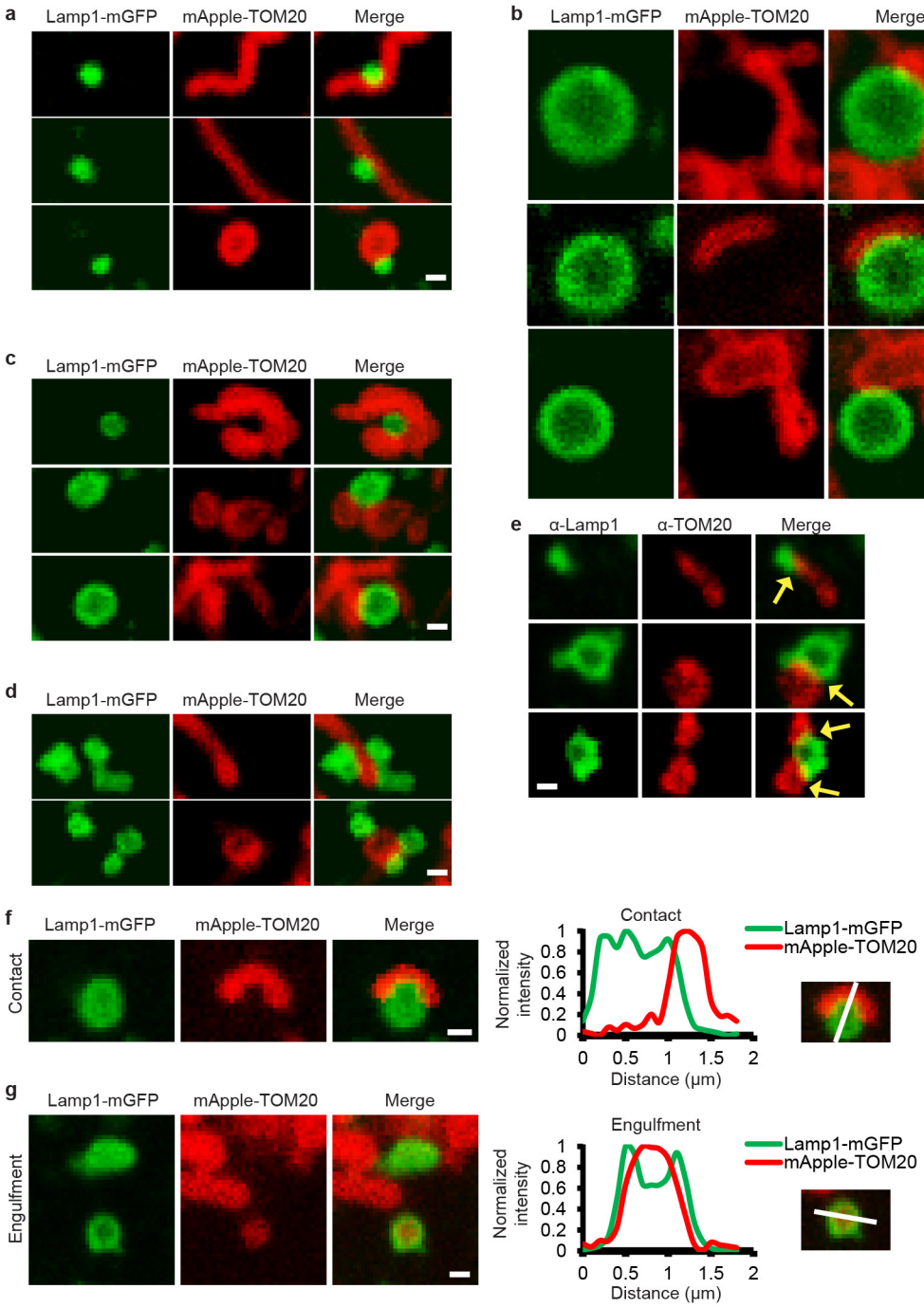

Extended Data Figure 2 | Characterizing mitochondria–lysosome contacts in living cells. a–d, Representative images of mitochondria–lysosome contacts (lasting more than 10 s) in living HeLa cells expressing LAMP1–mGFP (lysosomes) and mApple–TOM20 (mitochondria) ($n = 23$ cells). **a**, Examples of small LAMP1 vesicles (vesicle diameter $<0.5\,\mu m$) contacting mitochondria. **b**, Examples of larger LAMP1 vesicles (vesicle diameter $>1\,\mu m$) contacting mitochondria. **c**, Examples of a single LAMP1 vesicles contacting multiple mitochondria. **d**, Examples of multiple LAMP1 vesicles contacting a single mitochondrion. **e**, Representative images of contacts (yellow arrows) in fixed HeLa cells stained for endogenous LAMP1 (green) and TOM20 (red) ($n = 341$ examples from 25 cells). **f**, **g**, Representative images of living HeLa cells ($n = 23$ cells) expressing LAMP1–mGFP (lysosomes) and mApple–TOM20 (outer mitochondrial membrane) with corresponding linescans showing a mitochondria-lysosome contact at close proximity (**f**), distinct from lysosomal engulfment of mitochondrial TOM20 (**g**). All scale bars, $0.5\,\mu m$.

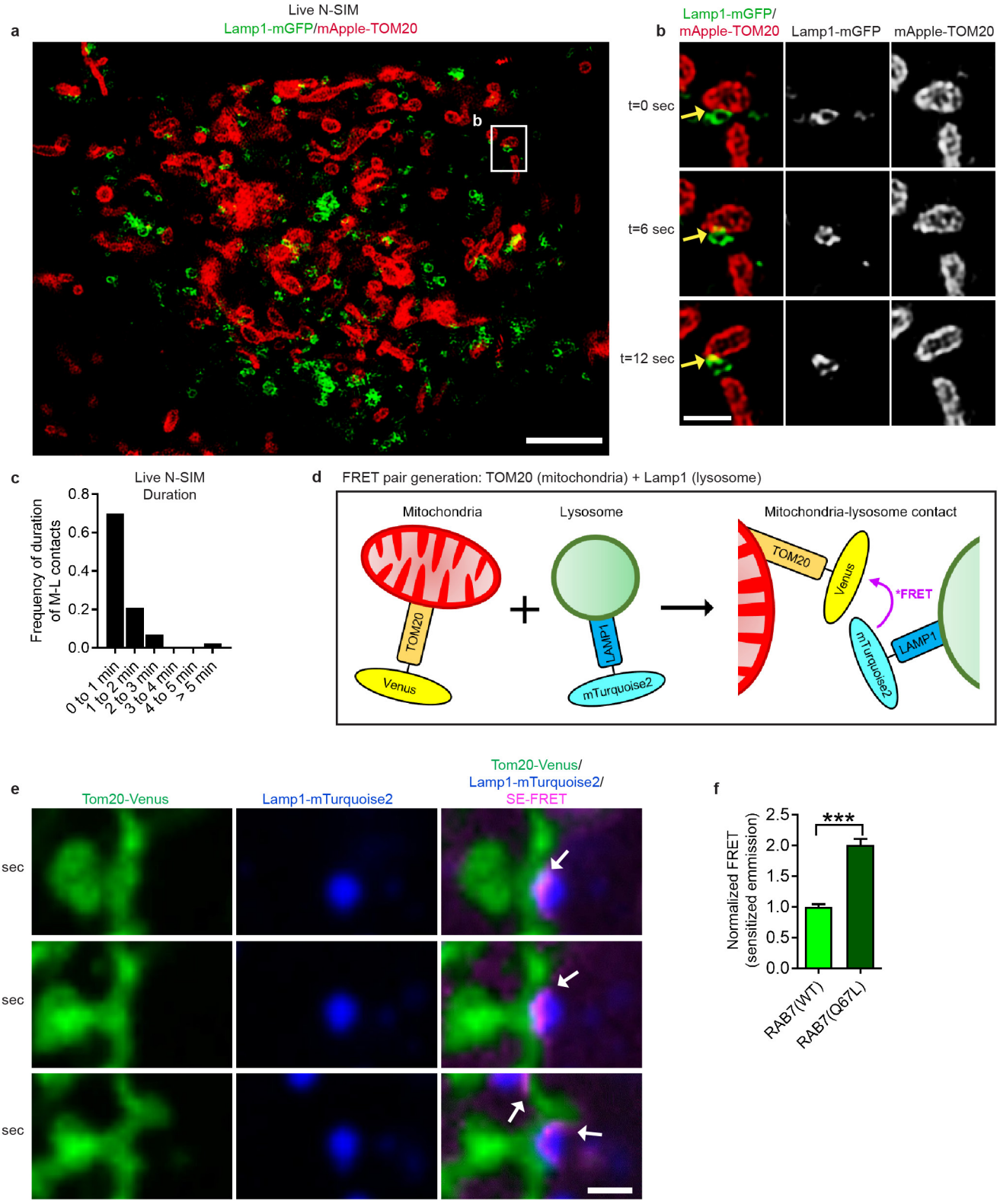

Extended Data Figure 3 | Structured illumination microscopy and FRET imaging of mitochondria–lysosome contacts in living cells. **a**–**c**, Representative N-SIM images (**a**, **b**) of mitochondria–lysosome contacts (yellow arrows) in living HeLa cells ($n = 43$ examples from 10 cells) expressing LAMP1–mGFP (lysosomes) and mApple–TOM20 (mitochondria) and quantification of duration of mitochondria–lysosome contacts from N-SIM time-lapse images (**c**). **d**, Model of newly generated FRET pairs targeted to the outer mitochondrial membrane (TOM20–Venus) and the lysosomal membrane (LAMP1–mTurquoise2). **e**, Representative time-lapse images of a living HeLa cell ($n = 200$ cells) expressing FRET pairs (TOM20–Venus, LAMP1–mTurquoise2) and RAB7a(Q67L)–mRuby3 demonstrating preferentially increased SE-FRET signal over 60 s at the interface between mitochondria and lysosomes (white arrows). **f**, Quantification of normalized SE-FRET intensity per cell in conditions expressing wild-type RAB7a or RAB7a(Q67L) ($n = 200$ cells per condition) showing an approximately twofold increase in cells expressing RAB7a(Q67L). Data are means ± s.e.m. $^{***}P < 0.0001$, unpaired two-tailed t-test (**f**). Scale bars, 4 μm (**a**); 1 μm (**b**, **e**).

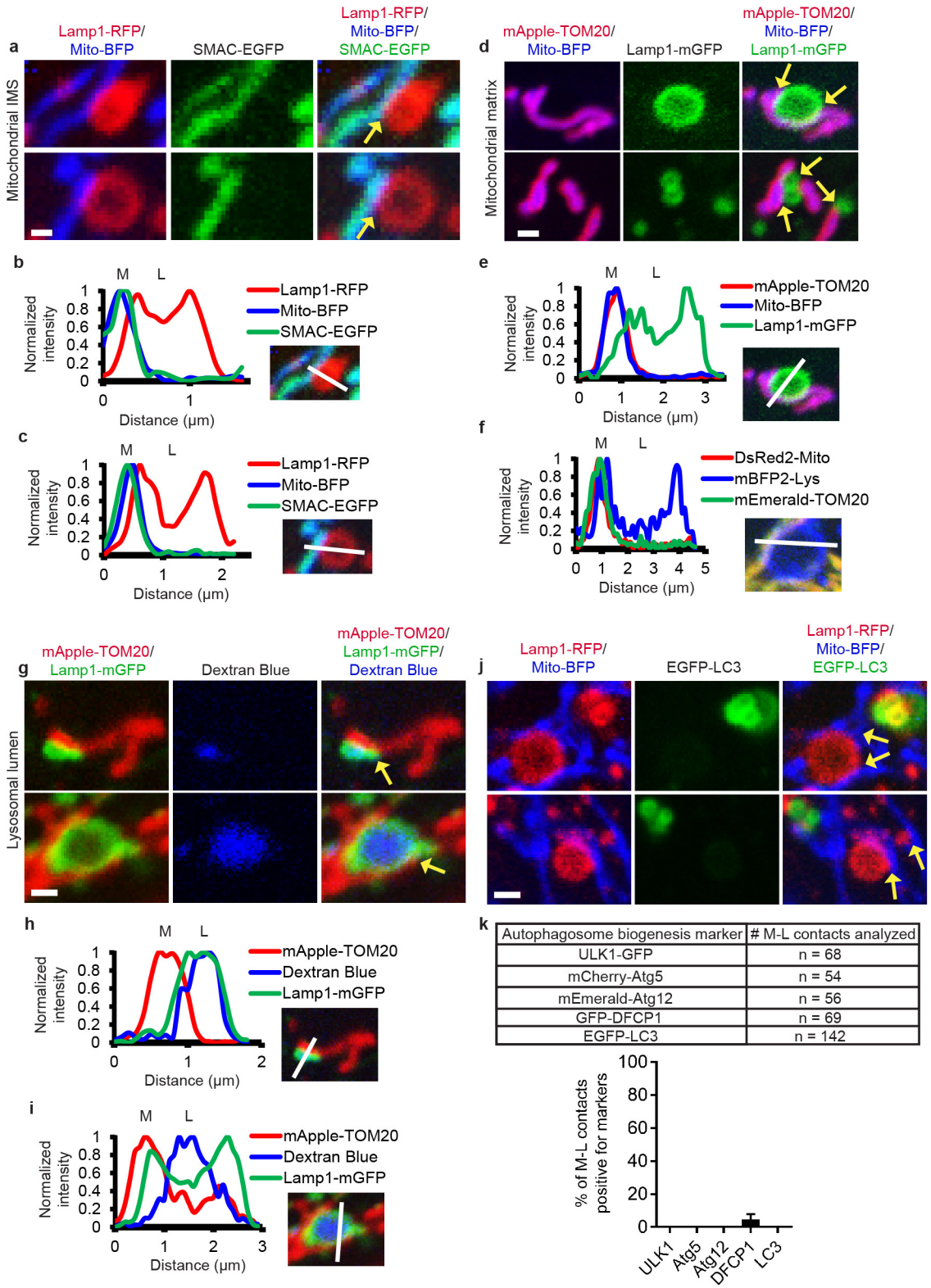

Autophagosome biogenesis marker	# M-L contacts analyzed
ULK1-GFP	n = 68
mCherry-Atg5	n = 54
mEmerald-Atg12	n = 56
GFP-DFCP1	n = 69
EGFP-LC3	n = 142

Extended Data Figure 4 | See next page for caption.

Extended Data Figure 4 | Mitochondria–lysosome contacts are distinct from mitochondria-derived vesicles and mitophagy. a–**c**, Representative images (**a**) of living HeLa cells expressing LAMP1–RFP (lysosomes), mito–BFP (mitochondrial matrix) and SMAC–EGFP (mitochondrial intermembrane space), and corresponding linescans (**b**, **c**) showing that mitochondrial intermembrane space and matrix proteins do not undergo bulk transfer into lysosomes at contacts (yellow arrows) ($n = 57$ events from 12 cells). **d**, **e**, Representative images (**d**) in a living HeLa cell expressing mApple–TOM20 (mitochondrial outer membrane), mito–BFP (mitochondrial matrix) and LAMP1–mGFP (lysosomes) and linescan (**e**, corresponding to top panel in **d**) showing that mitochondria that form contacts with lysosomes (yellow arrows) are positive for mitochondrial matrix protein mito-BFP and are not TOM20-positive MDVs ($n = 104$ events from 23 cells). **f**, Representative linescan in a living HeLa cell expressing mEmerald–TOM20 (mitochondrial outer membrane), DsRed2–Mito (mitochondrial matrix) and mBFP2–Lys (lysosomes) showing that mitochondria that form contacts with lysosomes are positive for mitochondrial matrix protein DsRed2–mito and are not TOM20-positive MDVs ($n = 94$ events from 16 cells). **g**–**i**, Representative images (**g**) in a living HeLa cell expressing mApple–TOM20 (outer mitochondrial membrane), LAMP1–mGFP (lysosomal membrane) and fluid-phase marker dextran blue pulse-chased into the lysosomal lumen, and corresponding linescans (**h**, **i**) showing that lysosomal luminal contents (blue) do not undergo bulk transfer into mitochondria at contacts (yellow arrows) ($n = 66$ events from 18 cells). **j**, Representative images in a living HeLa cell expressing LAMP1–RFP (lysosomes), mito–BFP (mitochondrial matrix) and EGFP–LC3 (autophagosome) showing that mitochondria that form contacts with lysosomes (yellow arrows) are not engulfed by autophagosomes (not undergoing mitophagy) ($n = 142$ events from 17 cells). **k**, Autophagosome biogenesis proteins (ULK1–GFP, mCherry–ATG5, mEmerald–ATG12, GFP–DFCP1 and EGFP–LC3) do not mark sites of mitochondria–lysosome contacts in living cells (number of events analysed in $n = 14$ cells (ULK1), $n = 17$ cells (ATG5, ATG12, LC3) or $n = 13$ cells (DFCP1), top; quantification, bottom). Mitochondria (M) and lysosomes (L) are indicated in linescans. Data are means ± s.e.m. Scale bars, 0.5 μm (**a**); 1 μm (**d**, **g**, **j**).

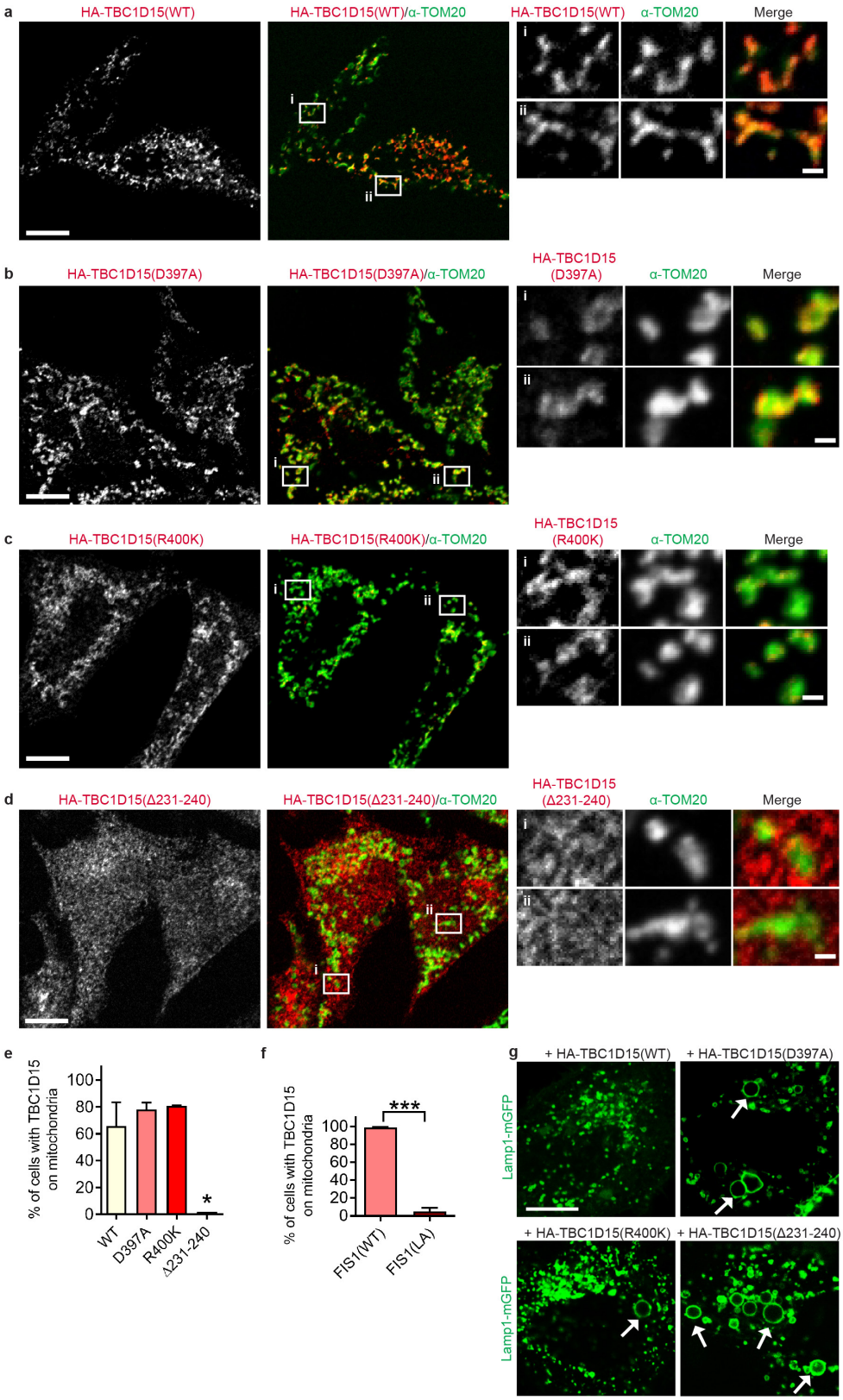

Extended Data Figure 5 | FIS1 recruits TBC1D15 to mitochondria. **a**–**e**, Representative images and quantification of localization of HA–TBC1D15 to mitochondria (stained with endogenous TOM20) in fixed HeLa cells showing that mitochondrial localization is not disrupted by TBC1D15 GAP mutants (D397A or R400K) but is disrupted by mutating the FIS1-binding site of TBC1D15 (Δ231–240) ($n = 293$ cells, WT; $n = 228$ cells, D397A; $n = 181$ cells, R400K; $n = 379$ cells, Δ231–240). Δ231–240 versus WT ($^*P = 0.0178$), D397A ($^*P = 0.0131$), and R400K ($^*P = 0.0112$), ANOVA with Tukey's post-hoc test. **f**, Quantification showing that localization of YFP–TBC1D15 to mitochondria is greatly decreased by the Flag–FIS1(LA) mutant (which cannot bind TBC1D15) as compared to wild-type Flag–FIS1 ($n = 290$ cells, FIS1; $n = 281$ cells, FIS1(LA)). $^{***}P < 0.0001$, unpaired two-tailed t-test. **g**, Examples of HA–TBC1D15 GAP mutants (D397A and R400K) or FIS1-binding mutant (Δ231–240) inducing enlarged lysosomes (white arrows) (LAMP1–mGFP) not observed in cells expressing wild-type HA–TBC1D15 ($n = 293$ cells, WT; $n = 228$ cells, D397A; $n = 181$ cells, R400K; $n = 379$ cells, Δ231–240). Data are means ± s.e.m. Scale bars, 10 μm (**a**–**d**, **g**); 1 μm (**a**–**d**, insets).

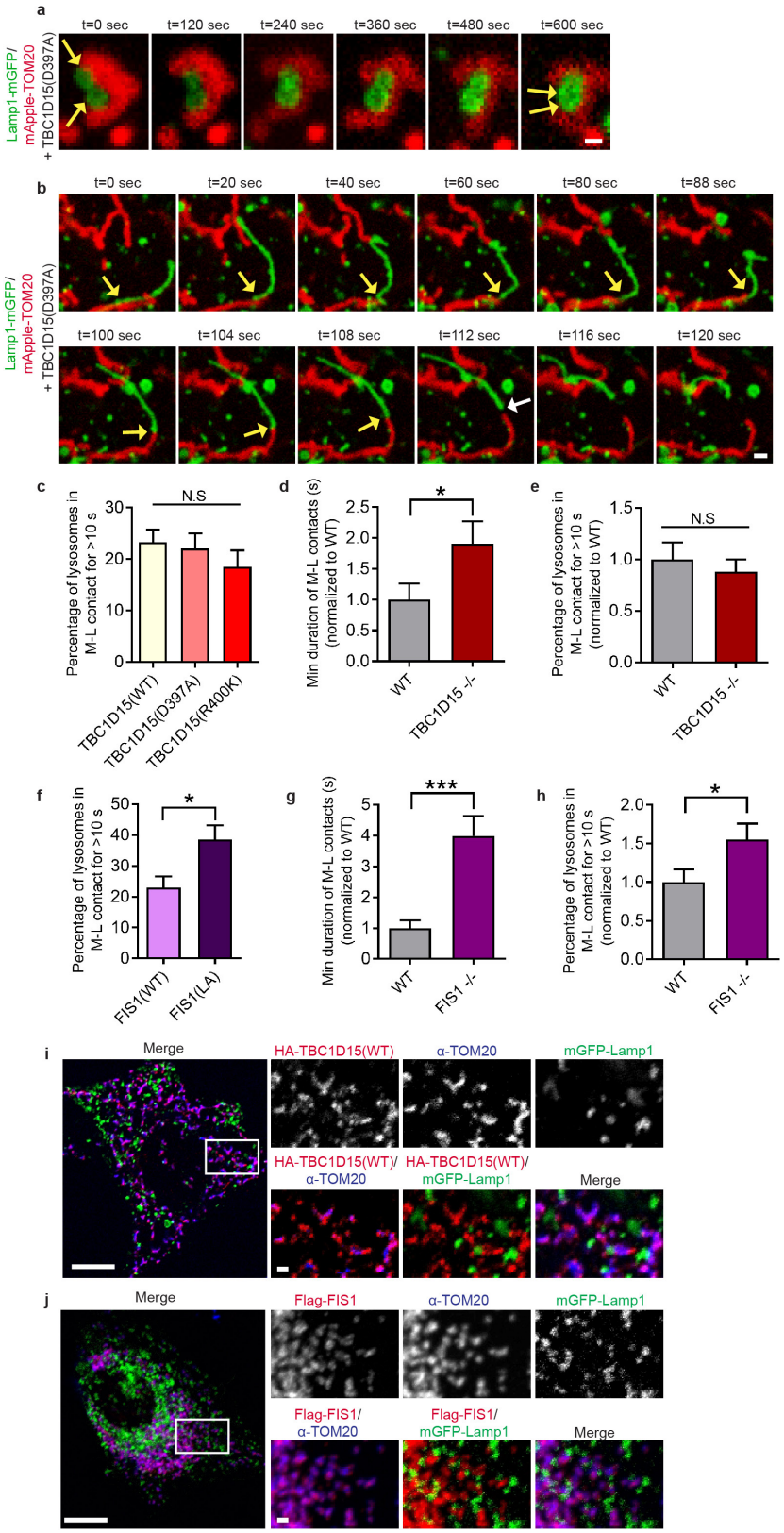

Extended Data Figure 6 | See next page for caption.

Extended Data Figure 6 | Recruitment of TBC1D15 by FIS1 to mitochondria promotes mitochondria–lysosome contact untethering. a, **b**, Representative time-lapse images of stable mitochondria–lysosome contacts (yellow arrows) for over 100 s before untethering (white arrow) in living HeLa cells expressing mApple–TOM20 (mitochondria), LAMP1–mGFP (lysosome) and the RAB7 GAP mutant TBC1D15(D397A) ($n = 38$ events from 10 cells). **c**, TBC domain mutants TBC1D15(D397A) and TBC1D15(R400K), which lack GAP activity, do not alter the percentage of lysosomes in contacts ($n = 12$ cells per condition), as compared to wild-type TBC1D15 (N.S., not significant). **d**, **e**, *TBC1D15*$^{-/-}$ HCT116 cells have increased duration (**d**, $n = 18$ events from 6 cells, WT; $n = 16$ events from 7 cells, *TBC1D15*$^{-/-}$) but no change in the number of mitochondria–lysosome contacts (**e**, $n = 15$ cells, WT; $n = 14$ cells, *TBC1D15*$^{-/-}$) compared to wild-type HCT116 cells ($^{*}P < 0.0491$, N.S., not significant). **f**, Expression of the Flag–FIS1(LA) mutant (unable to bind TBC1D15) increases the percentage of lysosomes in mitochondria–lysosome contacts compared to wild-type FIS1 in living HeLa cells ($n = 18$ cells, FIS1; $n = 16$ cells, FIS1(LA); $^{*}P < 0.0117$). **g**, **h**, *FIS1*$^{-/-}$ HCT116 cells have an increased duration (**g**, $n = 18$ events from 6 cells, WT; $n = 14$ events from 6 cells, *FIS1*$^{-/-}$) and number of mitochondria–lysosome contacts (**h**, $n = 15$ cells, WT; $n = 13$ cells, *FIS1*$^{-/-}$) compared to wild-type HCT116 cells ($^{*}P < 0.0442$, $^{***}P < 0.0001$). **i**, **j**, Localization of HA–TBC1D15 (**i**, $n = 293$ cells) and Flag–FIS1 (**j**, $n = 272$ cells) to mitochondria in fixed HeLa cells is not restricted to mitochondria–lysosome contacts. Data are means ± s.e.m. ANOVA with Tukey's post-hoc test (**c**), unpaired two-tailed *t* test (**d**–**h**). Scale bars, 0.5 μm (**a**); 1 μm (**b**, **i** (insets), **j** (insets)); 10 μm (**i**, **j**).

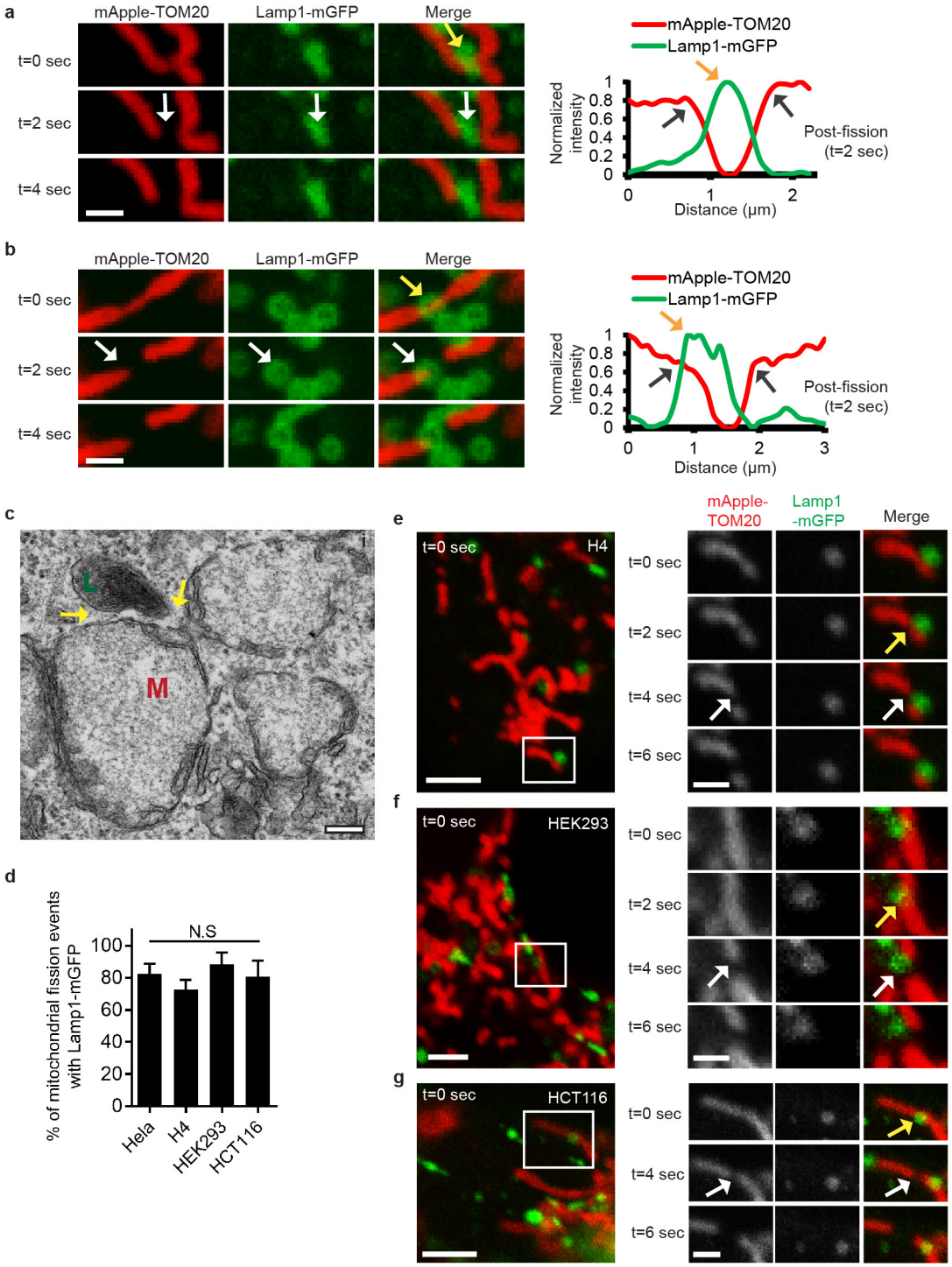

Extended Data Figure 7 | Mitochondrial fission sites are marked by mitochondria–lysosome contacts in multiple cell types. **a**, **b**, Representative time-lapse images of lysosomes contacting mitochondria at site of mitochondrial fission (yellow arrow, top) before mitochondrial fission (white arrows, middle) in living HeLa cells expressing mGFP–LAMP1 (lysosomes) and mApple–TOM20 (mitochondria) with corresponding linescans (right) showing lysosomes at the site of fission (yellow arrow; linescan) after mitochondrial division into two daughter mitochondria (grey arrows, linescan) ($n = 62$ events from 23 cells). **c**, Electron microscopy image of mitochondria (M) in contact (<30 nm) with a lysosome (L; yellow arrows) at site of mitochondrial constriction in untreated HeLa cells (from $n = 20$ cells imaged). **d**–**g**, Lysosomes (yellow arrows in **e**–**g**; mGFP–LAMP1) mark sites of mitochondrial fission (white arrows in **e**–**g**; mApple–TOM20) at similar rates (**d**) in living H4 neuroglioma, HEK293 and HCT116 cells as in HeLa cells by time-lapse confocal imaging ($n = 49$ events from 10 cells, HeLa; $n = 36$ events from 13 cells, H4; $n = 18$ events from 9 cells, HEK293; $n = 9$ events from 6 cells, HCT116). Data are means ± s.e.m. N.S., not significant, ANOVA with Tukey's post-hoc test. Scale bars, 1 μm (**a**, **b**, **e**–**g**, insets); 200 nm (**c**); 2.5 μm (**e**–**g**).

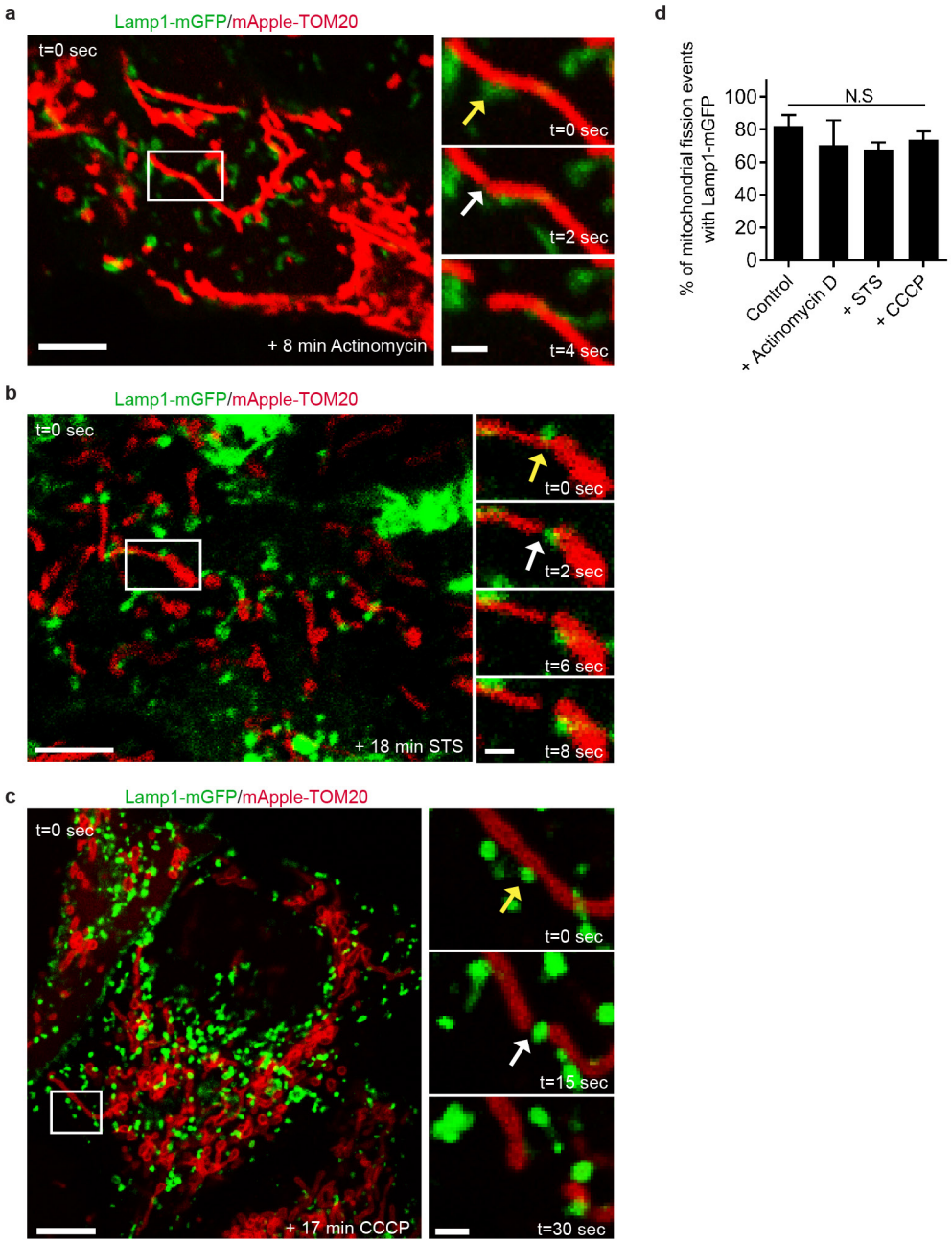

Extended Data Figure 8 | Mitochondria–lysosome contacts mark sites of mitochondrial fission upon induction of mitochondrial fragmentation. a–d, Lysosomes (yellow arrows; mGFP–LAMP1) mark sites of mitochondrial fission (white arrows; mApple–TOM20) at similar rates (**d**) in untreated living HeLa cells as in cells treated for up to 20 min with actinomycin D (**a**), STS (**b**) or CCCP (**c**) ($n = 49$ events from 10 cells, control; $n = 29$ events from 14 cells, actinomycin D; $n = 36$ events from 10 cells, STS; $n = 49$ events from 14 cells, CCCP). Data are means ± s.e.m. N.S., not significant, ANOVA with Tukey's post-hoc test. Scale bars, 5 μm (**a**-**c**); 1 μm (**a**–**c**, insets).

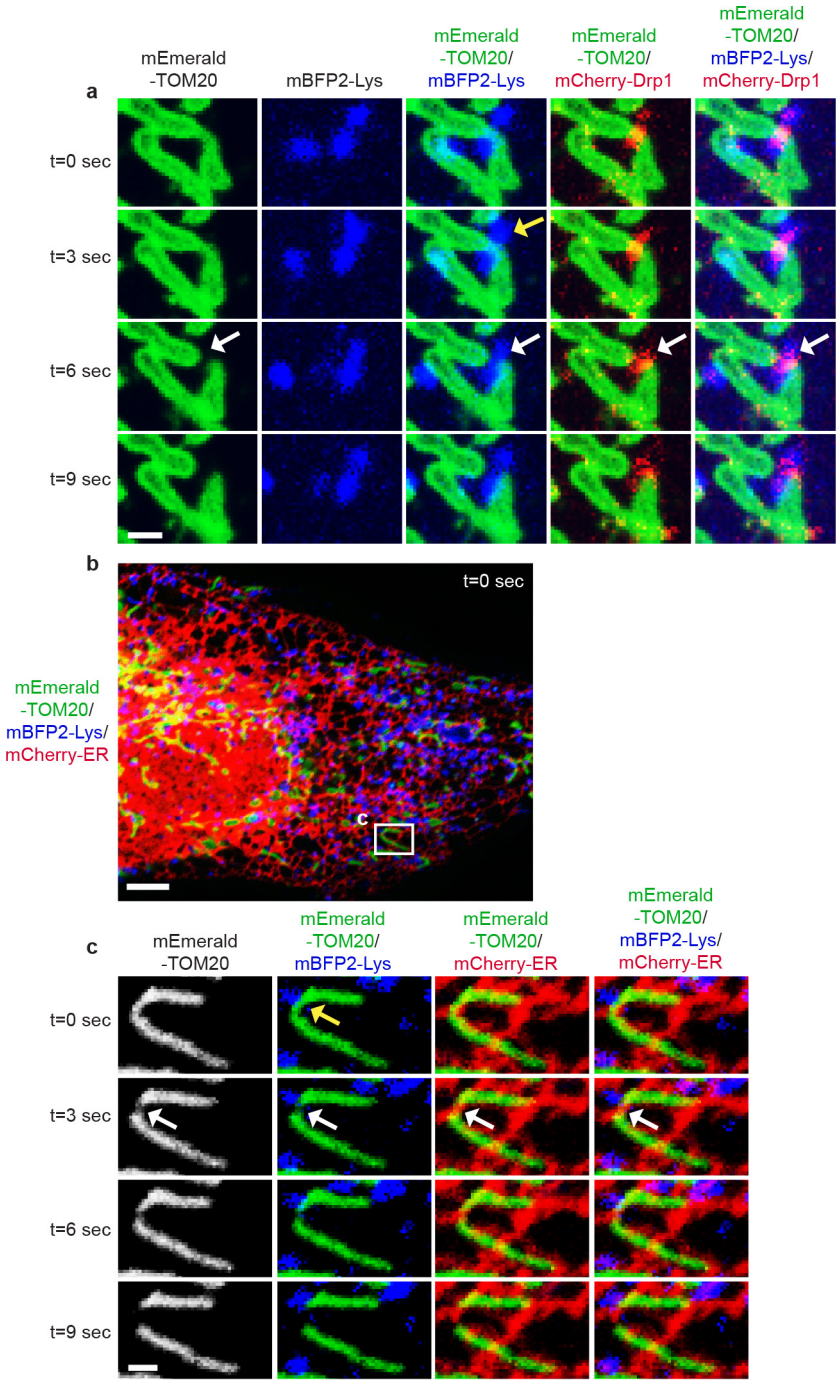

Extended Data Figure 9 | Mitochondrial fission sites marked by lysosomes are positive for DRP1 and endoplasmic reticulum tubules. **a**, Representative time-lapse images of a lysosome (mBFP2–Lys) contacting mitochondria (mEmerald–TOM20) at the site of mitochondrial division (yellow arrow) before fission (white arrows) in a living HeLa cell showing mCherry–DRP1 oligomerization at the site of mitochondrial division ($n = 41$ events from 11 cells). **b**, **c**, Representative image (**b**, inset time-lapse images shown in **c**) of a lysosome (mBFP2–Lys) contacting mitochondria (mEmerald–TOM20) at the site of mitochondrial division (yellow arrow) before fission (white arrows) in a living HeLa cell showing an endoplasmic reticulum tubule (mCherry–ER) at the site of mitochondrial division ($n = 54$ events from 16 cells). Scale bars, 1 μm (**a**, **c**); 5 μm (**b**).

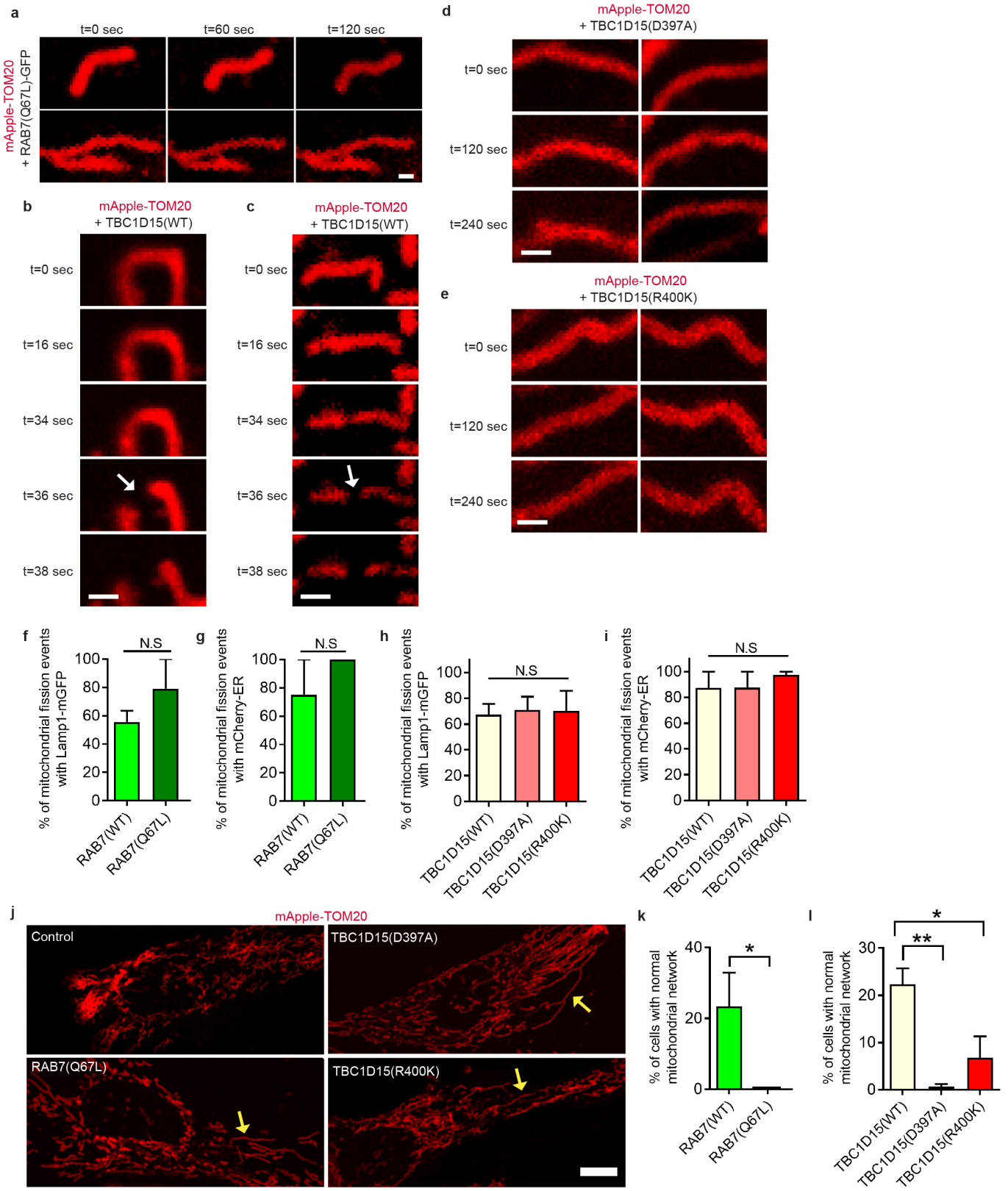

Extended Data Figure 10 | See next page for caption.

Extended Data Figure 10 | Regulation of mitochondrial network dynamics by RAB7 GTP hydrolysis. a, Examples of mitochondria not undergoing fission for more than 120 s in living HeLa cells expressing mApple–TOM20 (mitochondria) and RAB7(Q67L)–GFP ($n = 13$ cells). **b**, **c**, Examples of mitochondria undergoing fission (white arrows) after 36 s in living HeLa cells expressing mApple–TOM20 (mitochondria) and wild-type TBC1D15 ($n = 13$ cells). **d**, **e**, Examples of mitochondria not undergoing fission for more than 240 s in living HeLa cells expressing mApple–TOM20 (mitochondria) and GAP mutants TBC1D15(D397A) (**d**) or TBC1D15(R400K) (**e**) ($n = 13$ cells per condition). **f**–**i**, The percentage of mitochondrial fission sites marked by lysosomes (mGFP–LAMP1; **f**, **h**) or endoplasmic reticulum (mCherry–ER; **g**, **i**) is not disrupted by the RAB7(Q67L) GTP-hydrolysis-deficient mutant (**f**, **g**; $n = 12$ events from 15 cells) or by TBC1D15 GAP mutants (D397A or R400K) (**h**, **i**; $n = 22$ events from 10 cells, WT; $n = 17$ events from 19 cells, D397A; $n = 27$ events from 22 cells, R400K). **j**–**l**, Examples of RAB7(Q67L) and HA–TBC1D15 GAP mutants (D397A and R400K) inducing elongated mitochondria (**j**, yellow arrows; $>10\,\mu m$ length) compared to control cells, and quantification of RAB7(Q67L) (**k**; $^{*}P = 0.0321$) and HA-TBC1D15 GAP mutants (D397A and R400K) (**l**; $^{*}P = 0.0297$, $^{**}P = 0.0051$) leading to decreased percentages of cells with normal mitochondrial networks (no elongated mitochondria $>10\,\mu m$ length or hyperfused or tethered networks) ($n = 47$ cells, RAB7; $n = 72$ cells, RAB7(Q67L); $n = 88$ cells, TBC1D15 WT; $n = 168$ cells, TBC1D15(D397A); $n = 132$ cells, TBC1D15(R400K)). Data are means ± s.e.m. N.S., not significant; ANOVA with Tukey's post-hoc test (**h**, **i**, **l**), unpaired two-tailed *t*-test (**f**, **g**, **k**). Scale bars, 0.5 μm (**a**); 1 μm (**b**–**e**); 10 μm (**j**).

nature research

Corresponding author(s): Dimitri Krainc

☐ Initial submission ☐ Revised version ☒ Final submission

Life Sciences Reporting Summary

Nature Research wishes to improve the reproducibility of the work that we publish. This form is intended for publication with all accepted life science papers and provides structure for consistency and transparency in reporting. Every life science submission will use this form; some list items might not apply to an individual manuscript, but all fields must be completed for clarity.

For further information on the points included in this form, see Reporting Life Sciences Research. For further information on Nature Research policies, including our data availability policy, see Authors & Referees and the Editorial Policy Checklist.

Experimental design

1. Sample size

   Describe how sample size was determined.

   All sample sizes are listed in detail in the figure legends and main text. The number of cells imaged are consistent with previous live cell imaging studies (and from N≥3 independent experiments).

2. Data exclusions

   Describe any data exclusions.

   No data were excluded from the analyses.

3. Replication

   Describe whether the experimental findings were reliably reproduced.

   All data presented were from biological replicates. All attempts at replication were successful.

4. Randomization

   Describe how samples/organisms/participants were allocated into experimental groups.

   Aside from the strong premise for the proposed research, additional steps were taken to ensure rigor and reproducibility, as follows: 1) scientific questions were addressed using complementary technical approaches to ensure that the findings were robust; 2) for studies involving multiple different experimental conditions in the same cell line, studies were performed on cells originating from the same cell line batch.

5. Blinding

   Describe whether the investigators were blinded to group allocation during data collection and/or analysis.

   Whenever possible, experimenters were blinded to condition and examiner to exclude bias. For example, for our preliminary analyses, we asked other researchers who were either involved or not involved in the study to examine blinded samples for biological effects.

Note: all studies involving animals and/or human research participants must disclose whether blinding and randomization were used.

6. Statistical parameters

For all figures and tables that use statistical methods, confirm that the following items are present in relevant figure legends (or in the Methods section if additional space is needed).

n/a	Confirmed
☐	☒ The exact sample size (*n*) for each experimental group/condition, given as a discrete number and unit of measurement (animals, litters, cultures, etc.)
☐	☒ A description of how samples were collected, noting whether measurements were taken from distinct samples or whether the same sample was measured repeatedly
☐	☒ A statement indicating how many times each experiment was replicated
☐	☒ The statistical test(s) used and whether they are one- or two-sided (note: only common tests should be described solely by name; more complex techniques should be described in the Methods section)
☐	☒ A description of any assumptions or corrections, such as an adjustment for multiple comparisons
☐	☒ The test results (e.g. *P* values) given as exact values whenever possible and with confidence intervals noted
☐	☒ A clear description of statistics including central tendency (e.g. median, mean) and variation (e.g. standard deviation, interquartile range)
☐	☒ Clearly defined error bars

See the web collection on statistics for biologists for further resources and guidance.

Software

Policy information about availability of computer code

7. Software

Describe the software used to analyze the data in this study.	Statistics and graphing were performed using Prism 7 (GraphPad) software. All videos and images were assembled using ImageJ 1.51j8 (NIH).

For manuscripts utilizing custom algorithms or software that are central to the paper but not yet described in the published literature, software must be made available to editors and reviewers upon request. We strongly encourage code deposition in a community repository (e.g. GitHub). *Nature Methods* guidance for providing algorithms and software for publication provides further information on this topic.

Materials and reagents

Policy information about availability of materials

8. Materials availability

Indicate whether there are restrictions on availability of unique materials or if these materials are only available for distribution by a for-profit company.	All unique materials used are readily available from the authors or from standard commercial sources detailed in the Methods section.

9. Antibodies

Describe the antibodies used and how they were validated for use in the system under study (i.e. assay and species).	Lamp1 rabbit antibody (Sigma, L1418), Tom20 mouse antibody (BD biosciences, 612278), Flag rabbit antibody (Sigma, F7425), HA rabbit antibody (Cell Signaling, 3724S), HA mouse antibody (Cell Signaling, 2367S) and Alexa fluorophore-conjugated secondary antibodies from Molecular Probes (Invitrogen) were used. All antibodies have been previously validated for use in the system under study (immunofluorescence in mammalian cell lines).

10. Eukaryotic cell lines

a. State the source of each eukaryotic cell line used.	HeLa (ATCC), HEK293 (Life Technologies), HCT116 (from Richard Youle) and H4 cells (from Pamela McLean) were used. Further details are provided in the Methods section (Cell Culture and Transfection subsection).
b. Describe the method of cell line authentication used.	Cell lines were previously authenticated by cytochrome c oxidase subunit I (COI) and short tandem repeat (STR) testing.
c. Report whether the cell lines were tested for mycoplasma contamination.	Cells lines were tested negative for mycoplasma contamination.
d. If any of the cell lines used are listed in the database of commonly misidentified cell lines maintained by ICLAC, provide a scientific rationale for their use.	No commonly misidentified cell lines were used.

Animals and human research participants

Policy information about studies involving animals; when reporting animal research, follow the ARRIVE guidelines

11. Description of research animals

Provide details on animals and/or animal-derived materials used in the study.	No animals were used in this study.

Policy information about studies involving human research participants

12. Description of human research participants

Describe the covariate-relevant population characteristics of the human research participants.	This study did not involve human research participants.